*Revista Mexicana de Astronomía y Astrofísica*, **40**, 107–135 (2004)

# ON THE NATURE OF THE LBV/WR ECLIPSING BINARY SYSTEM HD 5980

G. Koenigsberger

Centro de Ciencias Físicas
Universidad Nacional Autónoma de México, Morelos, México

*Received 2004 February 6; accepted 2004 March 10*

RESUMEN

Se presenta un análisis del sistema multiple HD 5980 situado en la Nube Menor de Magallanes y de los efectos de la colisión entre los vientos, y se discute su posible ubicación en el diagrama H-R. Los datos analizados comprenden el período 1979-2002 y son consistentes con la clasificación original WNE de la estrella B, la compañera cercana de la estrella A que en 1993-1994 tuvo una erupción. La evolución del sistema probablemente se pueda describir utilizando trazas evolutivas que incluyan los efectos de rotación y/o el intercambio de masa.

ABSTRACT

HD 5980 is a multiple star system in the Small Magellanic Cloud that underwent a luminous blue variable-like eruption in 1993-1994. The erupting star (star A) forms part of a close eclipsing binary whose companion's (star B) Wolf-Rayet nature has recently been questioned. The data analyzed in this paper cover the period 1979-2002, and support the WNE classification of star B. The orbital phase-dependent variations of ultraviolet P Cygni absorption lines imply that the wind speed of star A is 1700–2200 km $s^{-1}$ and that of star B is 2600–3100 km $s^{-1}$. These allow an estimate of the wind-wind collision (wwc) shock cone geometry and line profiles from the wwc region. Given the assumed mass-loss rates, only a small fraction of the observed emission line profiles may originate in the wwc region. The star A+star B binary pair is likely the result of evolution with mass transfer and/or evolution with rapid rotation, and provides a magnificent opportunity for studying the processes that occur in massive multiple systems at the stages of stellar evolution just prior to the supernova event.

*Key Words:* **STARS: BINARIES (ECLIPSING) — STARS: INDIVIDUAL (HD 5980) — STARS: WINDS, OUTFLOWS — STARS: WOLF-RAYET — STARS: VARIABLES (LUMINOUS BLUE VARIABLES)**



## 1. INTRODUCTION

HD 5980 is the most luminous system in the Small Magellanic Cloud (SMC). It is associated with the largest SMC cluster, NGC 346, and lies within the giant H II region N66. Some of the earliest spectroscopic studies describe HD 5980 as a Wolf-Rayet (WR) star of the nitrogen sequence (WN) with a spectrum displaying very strong He II emission lines and superposed photospheric absorption lines presumed at that time to arise in a close binary companion.

Between 1993 and 1994, HD 5980 suffered an eruption (Bateson, Gilmore, & Jones 1994; Barbá et al. 1995; Koenigsberger et al. 1995), similar to the luminous blue variable (LBV) eruptive events. That is, its visual luminosity increased by $\sim 3$ magnitudes, and its spectrum developed strong and narrow emission lines of low ionization stages such as H I and He I, characteristics that in the LBV's are associated with enhanced mass-loss episodes. However, HD 5980 differs significantly from all the known LBV's except, perhaps, $\eta$ Carinae, which, however, is too enshrouded by dust to allow its stars to be characterized. One major difference with the other LBV's is that the erupting star in HD 5980 was relatively hot (WN6/7) shortly before it erupted. No known LBV has had a WN6 or WN7 progenitor. An additional peculiarity is that it is in an eclips-

TABLE 1

SUMMARY OF HIGH RESOLUTION UV DATA

| Epoch | Num. | $m_V$ | $F_{1850}$ | $F_{\rm N\ IV}$ | $F_{\rm He\ II}$ | $F_{\rm N\ V}$ | Comments |
|---|---|---|---|---|---|---|---|
| | | mag | $10^{-12}$ erg cm$^{-2}$ s$^{-1}$ | | | | |
| (1) | (2) | (3) | (4) | (5) | (6) | (7) | (8) |
| IUE | | | | | | | |
| 1978 | ··· | 11.7 | 1.73 | n.p.[a] | 33.8 | 13: | 1 low res. swp1598 |
| 1979 | 3 | 11.7 | 1.84 | n.p. | 39.9 | 30.9 | no $\phi$[c] $\sim 0.36$ |
| 1981 | 4 | 11.6 | 1.94 | n.p. | 53.0 | 31.1 | no $\phi$[c] $\sim 0.36$ |
| 1986 | ··· | 11.4 | 1.97 | 5.3: | 57.6: | 20: | 12 low res. only |
| 1989 | 4 | 11.3 | 2.07 | 15.3 | 80.0 | 23.2 | no $\phi \sim 0.0$ |
| 1991 | 6 | 11.4 | 2.10 | 15.6 | 82.7 | 22.9 | |
| 1994 | ··· | 10.1 | 3.30 | 2.: | 24: | 1:: | 1 low res. swp52824 |
| 1994 | 6 | 10.6−10.1 | 2.1−3.2 | 11-26 | 28-55 | $< 5.$ | |
| 1995a | 7 | 11.0−11.3 | 1.8−2.8 | 39.2 | 105.9 | 20.1 | |
| 1995b | 6 | 11.3 | 1.7−2.2 | 32.0 | 105.7 | 20.3 | |
| *HST*/STIS | | | | | | | |
| 1999 | 5 | n.a.[b] | 1.7−2.2 | 25.0 | 117.1 | 23.6 | |
| 2000 | 1 | n.a. | 2.04 | 17.9 | 98.7 | 28.2 | |
| 2002 | 1 | 11.3 | 1.82 | 12.2 | 78.8 | 20.7 | $m_V$ from S. Duffau |

[a]n.p. indicates "not present"; [b]n.a. indicates "not available"; [c]$\phi$ is orbital phase.



ing binary system and, furthermore, that the secondary component of the binary may also be a WN star. With the possible exception of $\eta$ Car, no other LBV+WR system is known.

The LBV class was originally defined by Conti (1984) and reviews may be found in Humphreys & Davidson (1994), Davidson, Moffat, & Lamers (1989), and Nota & Leitherer (1997). The LBV's are evolved massive stars subject to violent instabilities and episodes of large mass loss. Standard evolutionary scenarios (Langer et al. 1994; Maeder & Meynet 1987; Meynet & Maeder 2000) predict that after leaving the Main Sequence, a massive ($\sim$ 50 – 120 $M_\odot$) O-star evolves toward lower effective temperatures due to a rapid increase in its stellar radius. In this evolution, it is believed to reach an instability limit at which a phase of rapid and enhanced mass loss occurs, peeling off the remaining layers of H-rich surface and exposing the He-rich core. In general, at this stage the winds are expanding slowly (100–200 km s$^{-1}$) and relatively low effective temperatures are observed (7000–9000 K). Once the He-rich layers are exposed and the core He-burning phase initiates, the effective temperature rises rapidly and the star is in the WR phase of its evolution. WR stars possess extremely intense stellar winds ($\dot{M} \sim 10^{-5}\ M_\odot$ yr$^{-1}$, $v_\infty \sim$ 2000–3000 km s$^{-1}$) and strong abundance enhancements of He and other heavier elements. Most of the WR's lack H completely (see Massey 2003 for a review of massive stars in general). If HD 5980 is truly a LBV+WR system, then it is in a very advanced stage of evolution, and nearing the time of a supernova (SN) explosion. Thus, HD 5980 has the potential of providing one of the clearest insights possible into the conditions that prevail just prior to the SN event in a massive binary system. For example, are the stars rapid rotators? To what degree has mass transfer and rotation modified the evolutionary trajectories of its components? How will its mass mass-loss history affect the expansion of the SN ejecta in its earliest stages?

Answering some of these questions, however, requires knowledge of the fundamental parameters of the stars in the system. Because HD 5980 is in the SMC, the visual luminosity of the system is fairly well established. The mass determination, however, may be affected by the interaction effects within the close binary pair, since they produce emission-line profile variability and may severly distort the radial velocity curves. But without a better understanding of the wind characteristics of the stars, it is not possible to estimate the impact of interaction effects on the spectral lines. The objectives of this paper are to review and analyze our current understanding of

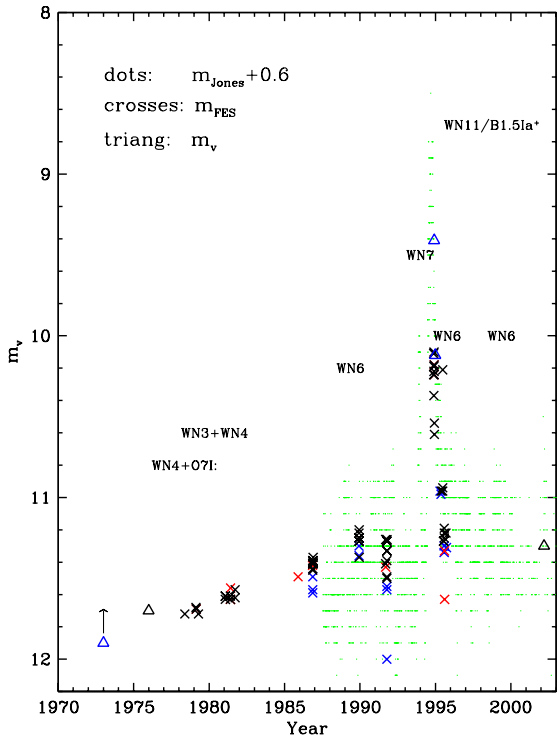


Fig. 1. Visual light curve of HD 5980 obtained by A. Jones (dots), Fine Error Sensor on IUE (crosses), and others (triangles). Spectral types corresponding to each epoch are indicated. The arrow indicates expected level out of eclipse.

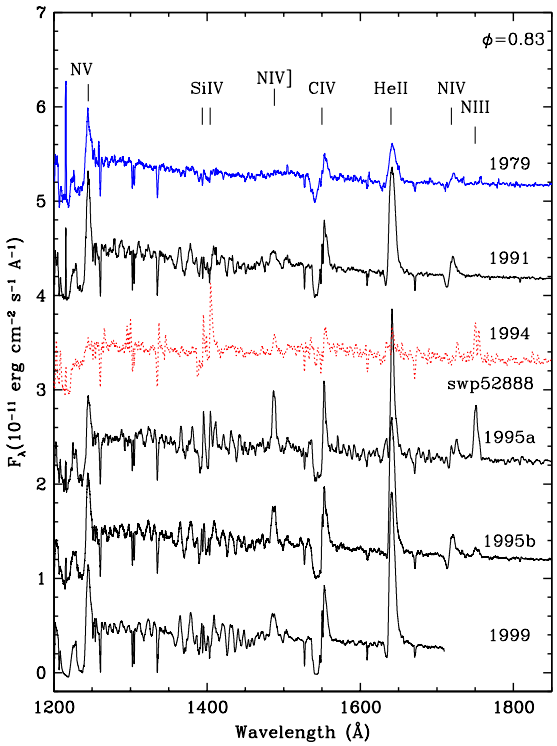


Fig. 2. Montage illustrating the long term changes in the UV spectrum of HD 5980 for spectra obtained at orbital phases near 0.83, except 1994 (dotted spectrum) which is at $\phi = 0.51$. A constant increment in vertical shift by 1 unit was made for display purposes.

HD 5980's characteristics, with an emphasis on the wind velocities within the system, and to address the question of the nature and evolutionary status of the stars composing the system.

## 2. OVERVIEW OF THE ERUPTIVE CYCLE

The data analyzed in this paper constitute the complete set of high resolution UV spectroscopic data between λλ1150–2000 Å obtained with the *International Ultraviolet Explorer Satellite* (IUE) and the *Hubble Space Telescope (HST)*. Details of the observations are described in de Boer & Savage (1980), Moffat, Koenigsberger, & Auer (1989), and Koenigsberger et al. (1994; 1998a; 1998b; 2000; Koenigsberger, Kurucz, & Georgiev 2002). Table 1 summarizes the general characteristics of these data, such as epoch of observation, number of spectra, average observed (i.e., not corrected for reddening) continuum flux at 1850 Å, and average observed flux contained within the principal emission lines. Low dispersion data of 1978 and 1986 are included in this table as they are the only available spectra for these epochs. Table 1 also lists the visual magnitudes obtained simultaneously with the corresponding UV data set, except for the value of 2002 which was obtained 1 month earlier. Due to the strong constraints for satellite observing time, orbital phase coverage is very incomplete in general, but particularly so in data sets prior to 1986, as noted in the last column of Table 1.

The possibility that HD 5980 was undergoing an outburst was first suggested by Koenigsberger et al. (1993), based on the changes detected in the UV data between 1979 and 1991. These changes can be summarized in terms of a gradual increase in line strengths, a decrease in line widths, and a decrease in the dominant degree of ionization in the spectrum. Because of their larger number, the optical observations provide the most detailed description of the evolving spectral characteristics prior to the eruption (Niemela et al. 1998). In the 1970's, HD 5980 was classified WN3-4; in the late 1980's it was WN6; in 1993 (just before the abrupt brightness increase) it had a WN7 classification. The few spectra available

at eruption indicate a spectrum similar to LBV's such as AG Car in its higher-temperature state (Barbá et al. 1995) or WN11 (Heydari-Melayari et al. 1997). The spectral types are correlated with the visual brightness: The spectrum is cooler for brighter visual magnitudes, although temperatures as low as typically observed in LBV outbursts have never been detected. Figure 1 summarizes the photometric data obtained between 1973-2002. The sources of these data are as follows: (1) Triangles prior to 1999 denote values from Azzopardi & Vigneau (1975), van den Bergh (1976), Massey, Parker, & Garmany (1989), and Koenigsberger et al. (1998b); in 1994 from Barbá et al. (1995); and the triangle in 2002 (2002 March 11) denotes a value obtained from CCD photometry kindly provided by S. Duffau (2002, private communication); (2) Crosses denote visual magnitudes that were obtained from the counts measured by the Fine Error Sensor (FES) on board the IUE and converted to a visual magnitude scale (Koenigsberger et al. 1998a); (3) Dots denote the visual magnitude estimates obtained and kindly provided by Albert Jones (1987 through 2003) with a correction of +0.6 mag as discussed by Breysacher (1997).

The data point of 1973 was obtained during an eclipse, and the arrow above this point indicates the expected brightness level of the system out of eclipse, assuming typical eclipse depths of $\Delta m_v \sim 0.26$ mag. Thus, Figure 1 shows that HD 5980 remained at $m_v \sim 11.7$ mag between 1973 and 1981, after which time it started to brighten. The range in FES $m_v$ values for 1986, 1989, and 1991 reflects variability due to the eclipses. The out-of-eclipse brightness for these epochs is $m_v \sim 11.3$ mag. Figure 2 illustrates typical UV spectra for seven epochs: 1979/81, 1989/91, 1994, 1995a, 1995b, 1999/2000, 2002, defined according to significant changes in the available data sets. In 1979/1981, the dominant features of the spectrum are the strong N V 1240, C IV 1550 and He II 1640 Å P Cygni emission lines, and weaker but prominent N IV 1718 Å. A weak O V 1371 Å P Cygni feature is also present. In 1989/1991, the spectrum contains a multitude of weaker emission lines attributable to Fe V and Fe VI, weak Si IV 1400 Å, and a now well-developed N IV] 1486 Å emission line. This line, arising from a semi-forbidden transition, is first observed in 1986 low-dispersion data. Assuming HD 5980 is comparable with the LMC R136 cluster WR's (see Crowther & Dessart 1998), the appearance of this line marks the transition from WN5 to WN6. Hence, the current active phase initiated between 1981 and 1986.

Unfortunately, no UV data exist just before or during the maximum of the eruption (between 1993 and mid-1994). The first high resolution UV spectrum, swp52888,[1] obtained during the declining branch of the eruption light curve displays narrow (FWHM 200−800 km $s^{-1}$) emission lines, most having P Cygni profiles, from ions such as C II, Fe II, Si III, N III, Al III as well as photospheric absorption lines similar to those present in the B1.5Ia$^+$ star HD 190603 (Koenigsberger et al. 1996). There is no sign of the N V 1240 Å emission line that was so prominent in previous epochs. By early 1995 (epoch 1995a), the spectrum displays very strong emission lines of N V, N Iv, He II, C IV, and the N III 1750 Å blend. All lines, except N V 1240 Å, are significantly stronger than prior to the eruption. The spectra of late 1995 (epoch 1995b) show a smooth transition into still greater emission-line fluxes in N IV] and He II, and broader lines.

The *HST* spectra (epochs 1999/2000 and 2002) provide the highest quality UV data available to date, and suggest that the trend for increasing emission line strengths may have continued until the year 2000.

A comparison between the spectra of 1979 (swp4277) and 1989 (swp37788) illustrating the numerous lines that developed by 1989 is shown in Figure 3a. Most of the strong lines at $\lambda < 1500$ Å are blends of Fe V and Fe VI. In Figure 3b, the same 1979 spectrum is compared with swp 52888 (1994), illustrating the narrow emission lines present during the descending branch of the eruption light curve, as well as the greatly enhanced UV continuum level.

## 3. THE STELLAR COMPONENTS IN THE HD 5980 SYSTEM

We now believe that at least three hot and luminous stars constitute the HD 5980 system: **star A** is a highly variable star whose wind structure is undergoing a transition, and part of this transition includes an LBV-like eruption; **star B** is the close companion ($P_{orb}$=19.2654 days), which was originally classified to be a WN3/4 star; and **star C** is an early O-type star. We adopt hereafter this nomenclature, first introduced by Barbá et al. (1996), to identify each of the three stars.

Hoffmann, Stift, & Moffat (1978) discovered HD 5980 to be an eclipsing binary, although the actual orbital period was found by Breysacher & Perrier (1980; henceforth BP80), and recently refined by Sterken & Breysacher (1997). The two eclipses

[1]SWP 52888 was kindly obtained by S. Shore on 1994 November 23.

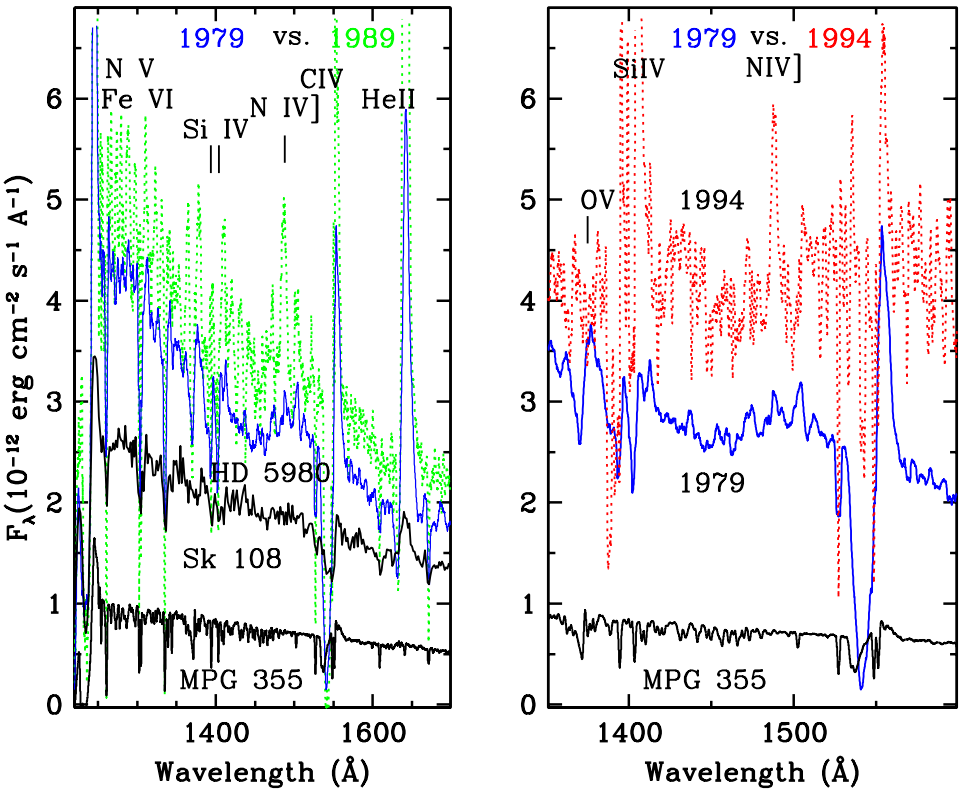


Fig. 3. Left: Spectra of HD 5980 obtained in 1979 (dark) and 1989 (dots) compared with the SMC binary system Sk 108 and the SMC star MPG 355(ON3III(f*) Walborn et al. 2000), illustrating the huge flux levels in HD 5980. The fluxes are not corrected for reddening, and no relative displacement has been introduced between the spectra. Right: Spectra obtained in 1979 (dark) and 1994 (dots) illustrating details of the changes in the spectrum.

were not separated equally in time: primary eclipse (star A "in front") at phase $\phi = 0.0$ and secondary (star B "in front") at $\phi = 0.36$, indicating an eccentric orbit ($e = 0.32$, Breysacher & Perrier 1991; $e = 0.27$, Moffat et al. 1998; $e = 0.30$, Kaufer et al. 2002). Figure 4 illustrates the geometry of the orbit of star A, in a reference frame centered on star B, corresponding to the parameters: $M_A$=50 $M_\odot$, $M_B$=28 $M_\odot$, $P$=19.265 days, $e$=0.27, and $\omega$=133°. The $x, y$ axes are in units of $R_\odot$, and the radius of star B is 15 $R_\odot$. The open squares are placed every 20° and the corresponding orbital phases are noted. The observer is located at the bottom of the figure.

The eclipse observed by BP80 at $\phi = 0.36$ was significantly broader than the primary eclipse, implying the presence of an extended and opaque region surrounding star B. Since the composite spectrum was clearly that of a WR star of the nitrogen sequence, star B was identified as the WN star, and the opaque region that produced the broad continuum eclipse was associated with its stellar wind. An analysis of the $V$-band light curve of the system in 1978 by Breysacher and Perrier (1991; henceforth, BP91) yielded values for the relative visual luminosities of the two stars: 41% (star A) and 29% (star B). The fact that the sum of luminosities did not equal 100% suggested the presence of a "third light" source (star C), and thus they reached the conclusion that the system is most likely formed by 3 stars. Niemela (1988) had already suggested that the system is triple (see below) and so had Massey et al. (1989), based on optical observations in which the image of HD 5980 was more extended than the expected point spread function for a point source. However, HD 5980 appeared as a point source on an *HST* image obtained with the WFPC2 in May 1994 (Proposal 5394, dataset U29T0101T, F255W, PI D. Welty), precluding the presence of a third object less than 3 mag fainter than HD 5980, at angular distances on the order of 0.1″, consistent with

the finding of Heydari-Malayeri et al. (1997) from sub-arcsecond adaptive optics observations.

Adopting $m_v$=11.7 mag, a reddening correction $a_\nu$=0.1 mag, a distance modulus to the SMC of 19.1 (Massey et al. 1989) and the relative luminosities given above, the absolute visual magnitudes of the three stars in 1978 are $V_A$=−6.5, $V_B$=−6.0, $V_C$=−6.3.

### 3.1. *Star C: the Third Component*

The UV luminosity of HD 5980 can easily accomodate contributions from three hot stars, as illustrated in Fig. 3a where the flux-calibrated spectra of HD 5980 in 1979 and 1989 are compared with the spectra of the binary system Sk 108 (WN4+O6.5I:), and the ON3III((f*)) star MPG 355 (Massey et al. 1989; Walborn et al. 2000). Sk 108 and MPG 355 are also located in the SMC. The sum of Sk 108 and MPG 355 observed fluxes reaches levels that are comparable to those of HD 5980 at $\lambda$ >1400 Å but are smaller at shorter wavelengths. Thus, assuming similar reddening corrections for the three systems, the continuum level in HD 5980 differs from the sum of three continua, WN4+O3V+O6.5I, only at the shortest wavelengths, at which HD 5980 is still brighter.

Photospheric absorption lines evident in the optical spectra of HD 5980 obtained prior to ∼ 1983 were originally thought to belong to star A (Breysacher, Moffat, & Niemela 1982; henceforth BMN82). However, data obtained in 1978-1983 yielded a radial velocity (RV) curve for these lines with a possible amplitude of no more than ∼ 50 km s$^{-1}$ (Moffat et al. 1998), much too small for the masses required by such luminous stars as star A and star B. Furthermore, Niemela (1988) showed that the N IV 4058 and N V 4603 Å emission lines moved in anti-phase. Since these lines arise only in stellar winds having large densities, she concluded that star A was also a WR star. The fact that the RV curve of the N V line followed star A's orbit implied a very hot spectral type for this star, WN3, and she concluded that the photospheric absorptions belonged to a third, line-of-sight object. In an analysis of the UV photospheric absorption lines of the *HST* UV spectra, Koenigsberger et al. (2002) found that the photospheric lines correspond to those of an O4-5 type star with a projected rotational velocity $v\ sin\ i$ ∼ 75 km s$^{-1}$ and that they do indeed have RV variations smaller than 30 km s$^{-1}$ over the 19-day orbit. They suggested the possibility that the ∼ 50 km s$^{-1}$ RV amplitude reported by Moffat et al. (1998) could be due to one of the following: (1) star C is itself a binary system; or (2) the spectrum of star C consists of strictly stationary absorption lines (at least over the orbital period of star A+star B), but these lines appear to undergo small-amplitude RV variations because they are superposed on very broad and variable photospheric absorptions associated with star A. Star A's absorptions would not be directly visible in the spectrum because of the strong (and variable) emission lines upon which they are superposed. Georgiev & Koenigsberger (2004a) showed the feasibility of the second possibility, concluding that star A could have a projected equatorial velocity, $v\ sin\ i \sim 230$ km s$^{-1}$. Peter Conti also suggested the possibility that the absorption lines consist of a blend of two contributions, one from a distant star and one from a star in the close orbit (see discussion summarized by Smith 1997).

In summary, the existence of star C is based on the "third light" of the eclipse light curve solution and on the presence of photospheric absorption lines that do not display large enough RV variations to be attributable to either star A or star B. The UV continuum flux levels are also consistent with this conclusion. It is yet to be determined whether star C is gravitationally bound to the A+B eclipsing binary, or whether it is simply a line-of-sight object. Koenigsberger et al. (1994) speculate that a gravitationally bound third star in the system could be responsible for perturbing stars A and B and producing the eruptive event; however, there has been no evidence for changes in the orbital parameters (Breysacher 1997). Hence, for the remainder of this paper we shall assume that star C is an O4-6 star whose only contribution to the spectrum is its continuum energy distribution, photospheric absorption lines, and UV emission lines typical of its spectral type (probably similar to MPG 355, illustrated in Fig. 3). This conclusion does not exclude the possibility of still additional unresolved stars along the line-of-sight to HD 5980, or that star C is itself a binary system. For example, Villar-Sbaffi, Moffat, & St.-Louis (2003) have suggested the presence of a collapsed companion in orbit around star B. If such a collapsed object were associated with HD 5980, it would not contribute significantly to the UV/optical continuum spectral energy distribution, nor to the photospheric absorption lines.

### 3.2. *Star A and its Eruption*

#### 3.2.1. *Evidence Pointing to Star A as the Eruptor*

The evidence pointing to star A as the eruptor is based on: (1) the appearance of a number of emission lines prior to the time of the eruptive event, their systematically increasing intensity, and their

RV variations which are consistent with the expected orbital motion of star A; (2) the increase in its radius after eruption, implied by changes in the visual lightcurve; and (3) the H-abundance inferred from the stellar wind lines near the time of the eruption.

As mentioned above (§ 3.1), Niemela (1988) found that the N V 4303,21 Å emission line RV data of the late 1970's followed the orbital motion of star A, as opposed to the N IV 4058 RV data which followed star B. The semi-amplitudes of the RV curves, $K_{N\ V} \sim 128$ and $K_{N\ IV} \sim 226$ km s$^{-1}$, allowed Niemela et al. (1997) to estimate the masses of the two stars, $M_A \sim 50\ M_\odot$ and $M_B \sim 28\ M_\odot$. After 1983, the N IV 4058 line no longer presents RV variations, a fact that can be explained if star A by then also contributes to the emission. More recently (1996, 1999) this line is found to follow the orbital motion of star A (Niemela et al. 1998; Kaufer et al. 2002), indicating the predominance of star A's emission lines. In the UV, the N IV] 1486 emission line and the Fe V/VI lines follow, in general, the orbital motion of star A (Koenigsberger et al. 1998a). The majority of these lines are not present pre-1986. This leads to the conclusion that star A developed an increasingly more massive stellar wind in the early 1980's, leading to a richer emission-line spectrum.

The pre-eruption light curve of the system (BP 1980; 1991) displays a sharp minimum centered at orbital phase $\phi$=0.0. This minimum has become much broader in the post-eruption light curve (Breysacher 1997), leading to the conclusion that star A (which is "in front" at $\phi$=0.0) has increased its radius.

The H-content deduced from the spectrum has also changed since the late 1970's. Koenigsberger et al. (1998b) estimated N[He]/N[H] $\sim$ 0.4 (by number) from post-eruption (1994) spectra while the pre-1980's spectra appear to be consistent with an absence of H. [2] Large post-eruption H-abundances were also found by Barbá, Niemela, & Morrell (1997) and Drissen et al. (2001). This leads to the conclusion that the pre-1980's He II emission line spectrum is produced by a wind having a negligible H-abundance (assumed to be that of star B) while the spectra of subsequent epochs are dominated by the wind with a larger H-abundance (star A). Evidence for the presence of some H as early as 1986 January is noted by Niemela, Barbá, & Morrell (1998), consistent with the notion that the enhanced activity phase of HD 5980 initiated prior to 1986.

[2]The H-abundance estimate for pre-1980, however, is based on published equivalent width values of H-Balmer lines and He II, and needs to be corroborated with a model-atmosphere fit to the spectrum.

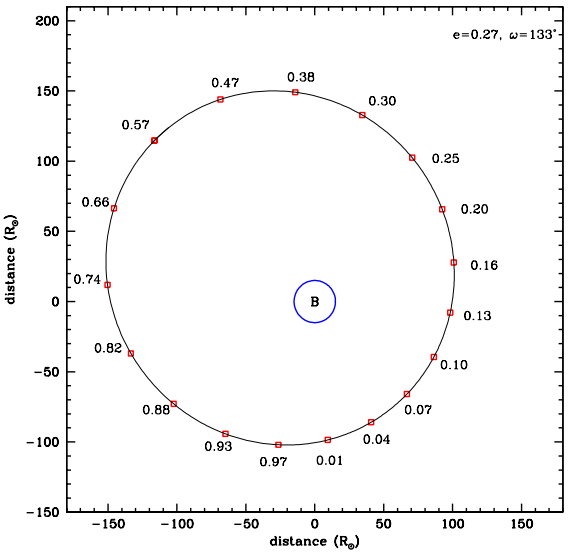


Fig. 4. Representation of the orbit of **star A** in a reference frame that is fixed with respect to **star B**. The observer is at the bottom. The open squares are located at 20° intervals and the corresponding orbital phases are listed.

The large H-abundance in star A is, however, somewhat puzzling because the WNE's in general are known to be very H-poor. On the other hand, there are no WNL's in the SMC, and it is possible that star A is an SMC analogue of Galactic WNL's but whose spectroscopic characteristics differ due to the lower heavy-element abundances.

Breysacher & Westerlund (1978; data of 1975-77) report strong He II photospheric absorption and weak or nearly absent He I, while Walborn (1977; data of 1973) reports strong He I but only a trace of He II. This suggests possible changes in the photospheric spectrum which may be associated with star A, indicating changes in its effective temperature in the 1970's. If such instabilities are related to the eruptive phenomenon this would indicate that the timescale for the growth of the instability is at least 30 years.

### 3.2.2. *Characteristics Near the Eruption Maximum*

According to the visual light curve of Jones & Sterken (1997), the eruptive phase of HD 5980 initiated with a precursor ($\Delta m_v \sim 1.4$ mag) eruption that occurred between 1993.8 and 1994.1 ($\sim$ 150 days). The second and more pronounced eruption

initiated in 1994.5, reaching maximum visual brightness $\sim$ 40 days later ($\Delta m_v \sim 2.5$ mag). The decline started in $\sim$ 1994.7 and the light curve leveled off at $m_v \sim 11$ mag by 1995.4. Thus the duration of this second event was $\sim$ 330 days. These features are illustrated in the amplified portion of the Jones light curve that is shown in the lower panel of Figure 5. UV lightcurve information is available only starting in 1994.8 (top of Fig. 5). It follows the declining trend of the visual light curve, but displays more structure. It first declines sharply by 0.6 mag in $\sim$ 30 days, after which it brightens slightly, and then continues the gradual decline with the same slope as the visual light curve.

Koenigsberger et al. (1996) find that SWP 52888, the fist post-eruption UV spectrum, is similar to that of a B1.5Ia$^+$ star (HD 190603), based on the similarity of Si III 1300, C II 1335, and Al III 1854,62 P Cygni features. This suggests an effective temperature $\sim$ 21,000 K which is similar to the 23,000 K determined by Drissen et al. (2001) from a NLTE model fit to a spectrum obtained by Heydari-Malayeri et al. (1997) in September 1994. However, there are important differences between swp52888 and the spectrum of the B1.5Ia$^+$ star HD 190603 (swp1822). In particular, the strength and width of Si IV 1393, 1402 (Figure 6) are far greater than in any B1 supergiant in the Walborn et al. (1980) Atlas, with the exception of the star $\epsilon$ Ori. Even the LBV AG Carinae does not display such strong Si IV P Cygni lines. Another important feature is that the P Cygni absorptions arising from lines of lower ionization (Si II – Al III) have slower edge velocities (300–860 km s$^{-1}$) than do the lines of Si IV and C IV, whose maximum velocities are $\sim$ 1700 km s$^{-1}$. These features are illustrated in Figure 7.

It is noteworthy that the low ionization P Cygni absorptions have line profiles very similar to those observed in the B1.5Ia$^+$ star, implying a similar wind velocity structure. That is, the line appears to be formed in a radially expanding wind, with velocity increasing outward, which excludes the possibility that the slow velocities correspond to a shell of "fossil" wind ejected during the eruption and expanding at the corresponding constant terminal velocity. On the other hand, this scenario does provide a potential explanation for the extended Si IV and C IV P Cygni absorptions. That is, the absorptions of Si IV and C IV within the range $-900$ and $-1750$ km s$^{-1}$ may be the signature of the "fossil" wind that left the star during the phases just prior to the rise to maximum. This wind would be expanding at constant velocity, and thus the width implies the superposition

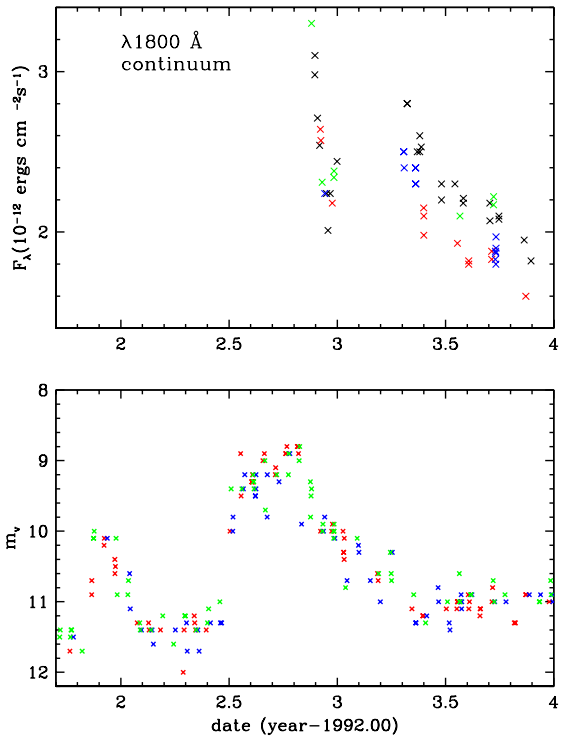


Fig. 5. Amplified portion of the visual light curve shown in Fig. 1 (bottom) and UV continuum flux levels at 1850 Å (top) during the descending branch of the 1994 eruption.

of multiple shells, each expanding with successively slower velocities. Such a stratified wind would be the result of sudden changes in the wind structure. Indeed, evidence for abrupt changes in the wind velocity may be found in the profiles of Si IV 1393 and 1402 Å. Each member of the doublet has a strong emission line and two P Cygni-like absorption components, one of which extends to $\sim$ 800 km s$^{-1}$ and the second one to 1750 km s$^{-1}$. The two absorptions are separated by what appears to be an emission line (FWHM $\sim$ 200 km s$^{-1}$). Three additional weaker emission-like features lie at $-1200$, $-1340$, and $-1500$ km s$^{-1}$ (Koenigsberger et al. 1995), as illustrated in Figure 8. These features are reminiscent of the absorption-line splitting that is observed to be particularly pronounced in LBVs such as R127 and AG Car (Stahl et al. 1983; 2001). As pointed out by Stahl et al. (2001), these regions of "missing absorptions" (or discrete emissions) indicate lower densities at the corresponding expanding velocities, suggesting that the wind changed abruptly from a

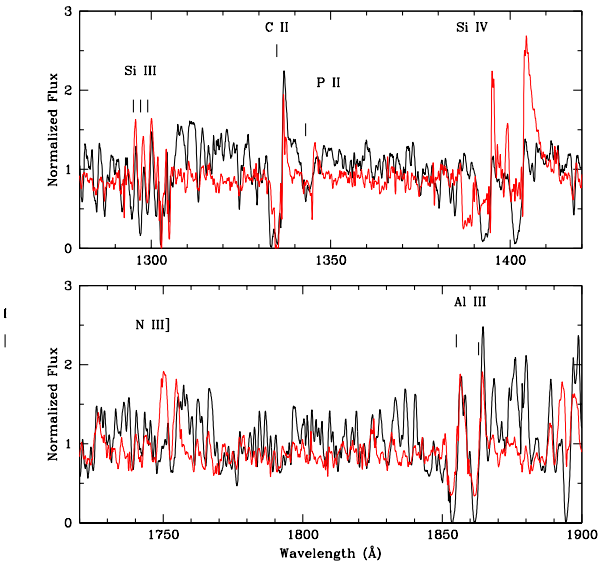


Fig. 6. Comparison between spectrum swp52888 (1994; $\phi$=0.51; light tracing) and the B1Ia$^+$ spectrum (swp1822). Both spectra are normalized to the continuum level.

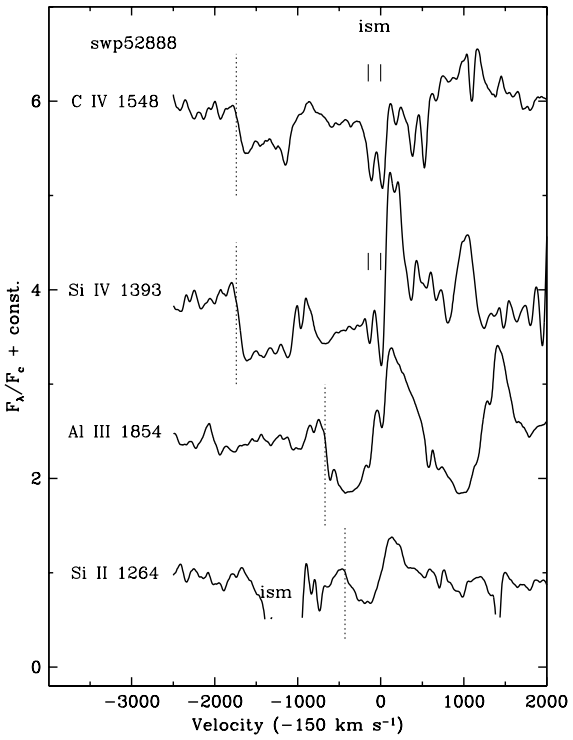


Fig. 7. Line profiles in swp 52888 as a function of velocity, corrected for the SMC motion. Vertical lines indicate $v_{edge}$=−1700, −670, and −430 km s$^{-1}$.

faster terminal speed to a slower one, leading to a shell of lower density between the two states.

The question is whether a signature of the pre-eruption wind may still be visible over the $\sim$ 1 year timescale implied by the observation of the Si IV features in swp52888. That is, from Fig. 5 the $\sim$ 1700 km s$^{-1}$ wind in question could have emerged from the system in 1993.7 or 1994.2. The spectrum swp52888 was obtained in 1994.9, the fossil wind thus having expanded out to 90,000 or 51,000 $R_\odot$, respectively. The total column density of gas along the line-of-sight to HD 5980 due to this wind is:

$$N_{col} = \frac{\dot{M}}{4\pi\mu m_H v_\infty} \int_{r_0}^{\infty} \frac{dr}{r^{-2}}\,, \qquad (1)$$

where $\dot{M}$ is the mass-loss rate, $\mu$ is the mean moleclar weight, $m_H$ is the mass of hydrogen, $v_\infty$ is the terminal wind speed, and $r_0$ is the inner radius of the expanding shell. After integration, this can be re-written as:

$$N_{col} = 2.7\times10^{23} \frac{\dot{M}_4}{\mu(r_0/100\ R_\odot)(v_\infty/1700\ \mathrm{km/s})}\ \mathrm{cm}^{-2}\,, \qquad (2)$$

where $\dot{M}_4$ is the mass-loss rate in units of $10^{-4}$ $M_\odot$ yr$^{-1}$. Typical Si abundances are log(Si/H) $\sim$ −4.5 and most of the Si in the WN7-like spectrum of star A just before the eruption is expected to be in the Si III and Si IV ionization stages. However, allowing for recombination, and considering a worst-case scenario, let us assume that N(Si IV)/N(Si) $\sim 10^{-2}$. Finally, assuming that the fossil 1700 km s$^{-1}$ wind was emitted in 1993.7, and assuming $\mu \sim 1$ we obtain $N_{col}^{Si\ IV} \sim 9\times10^{13}$ cm$^{-2}$. This is similar to the column density obtained for the interstellar medium Si IV lines in the SMC along the line-of-sight to HD 5980 by Savage & de Boer (1981) and Koenigsberger et al. (2001) and thus, renders plausible that a fossil wind with the above-mentioned characteristics would be detected spectroscopically, as appears to be the case.

If we assume that the emission-like features in HD 5980 are indeed due to lower densities in the corresponding wind velocities and that they represent times at which the wind terminal velocity changed, we are led to a scenario in which star A underwent at least four distinct episodes of decreasing wind speed just prior to eruption maximum. It is tempt-

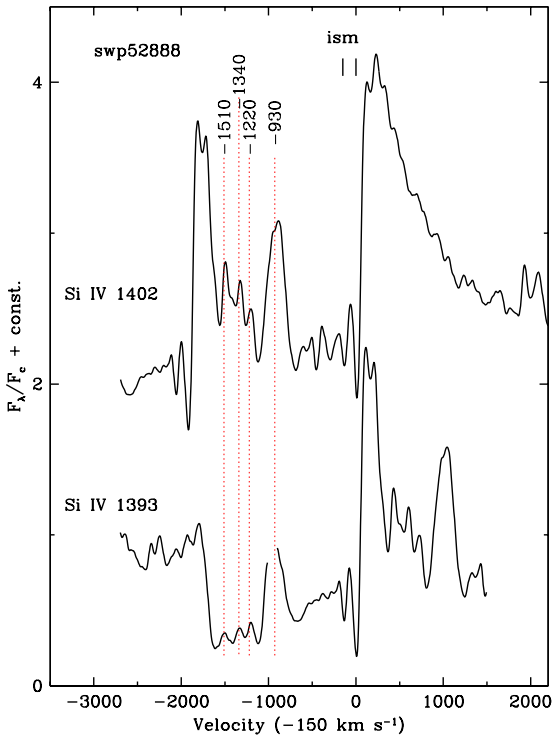


Fig. 8. Si IV 1393 and 1402 on a velocity scale, illustrating the discrete "emissions" located at −930, −1220, −1340, −1500 and possibly −1810 km s$^{-1}$. The emission at −930 is still present 38 days later.

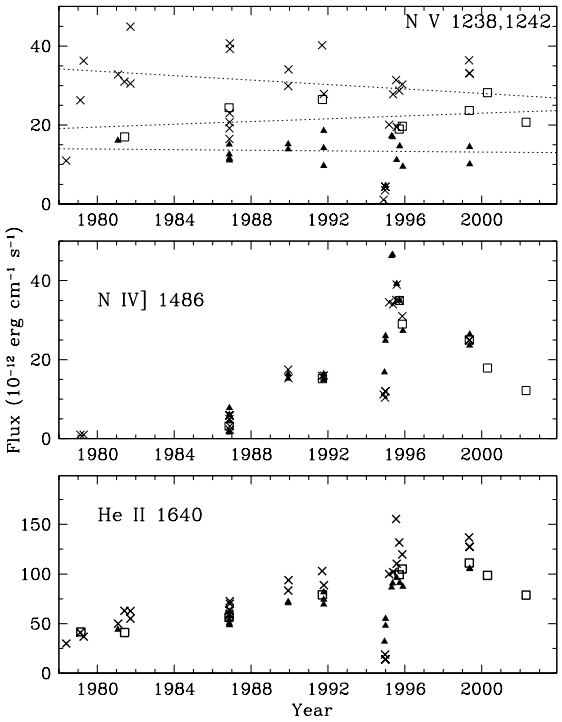


Fig. 9. The flux contained in the N V 1238,1240, N IV] 1486, and He II 1640 Å emission lines. Squares represent orbital phase $\phi = 0.0 \pm 0.08$; triangles are $0.25 < \phi < 0.50$, and crosses are at the other phases. The dotted lines in the top panel are least squares fits to the data for each of the phase intervals given above, but excluding data of epoch 1994.

ing to suggest that the jumps are associated with the orbital cycle, and that the trigger for each abrupt change in wind speed is the periastron passage. This hypothesis would establish the timescale over which each velocity persisted and, hence, the optical depth to be computed. This also leads to the conclusion that $v_\infty$(A) $\sim$ 1750 km s$^{-1}$ just before the eruption.

Contemporaneous visual and UV observations were made on 1994 December 30/31 (Koenigsberger et al. 1998b; swp53216 and 53226). The visual spectrum at this time was completely dominated by the erupting star, allowing a determination of mass-loss rate, luminosity and temperature of star A. Assuming a homogeneous, spherically symmetric wind distribution, the inferred mass-loss rate is $\dot{M}$ $\sim 10^{-3}$ $M_\odot$ yr$^{-1}$, similar to the value obtained by Drissen et al. for data acquired in September of the same year. Assuming that the mass-loss rate was sustained between 1993.8 (start of the precursor eruption) and 1995.4, the system may have lost up to $1.6\times10^{-3}$ $M_\odot$ in this single event.

### 3.2.3. *Post-Eruption Characteristics*

The visual brightness of star A reached a maximum during the 1994 eruption, but the intensity of He II 1640 Å and N IV] 1486 Å lines continued to increase after the eruptive event, reaching maximum values around epoch 1995b. Figure 9 shows the values of observed flux[3] contained within the emission lines of N V 1240, N IV] 1486, and He II 1640 Å as a function of date, from data listed in Table 2. Different symbols represent different orbital phases: squares ($0.92< \phi <1.08$), triangles ($0.25< \phi <0.50$), and crosses ($0.08< \phi <0.25$; and $0.50< \phi <0.90$). The peak intensities of N V 1240 and He II 1640 Å saturated the IUE detector in data obtained after 1981, so these data are lower limits. The

[3]Using absolute flux values (as opposed to equivalent widths) has the advantage of providing unambiguous information on the variability of the line strengths, independent of the variations in continuum flux levels.

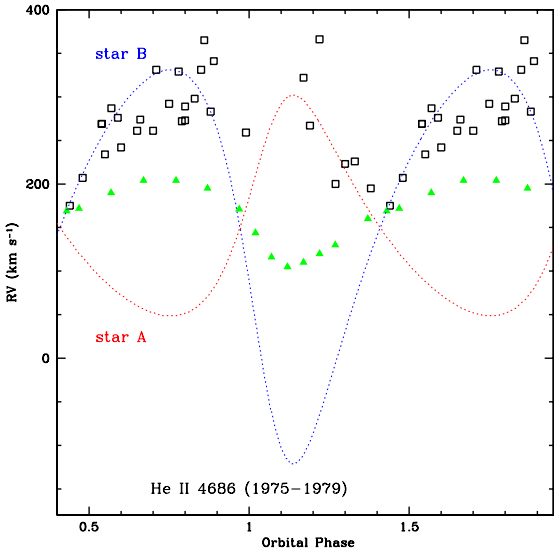


Fig. 10. Orbital phase-dependent RV variations of He II 4686 Å data from BMN82 (open squares) and the predicted RV variations (triangles) obtained if one assumes that both stars emit He II 4686 in their stellar winds with no interaction effects. The RV curves from Niemela et al. (1997) of both stars are also illustrated.

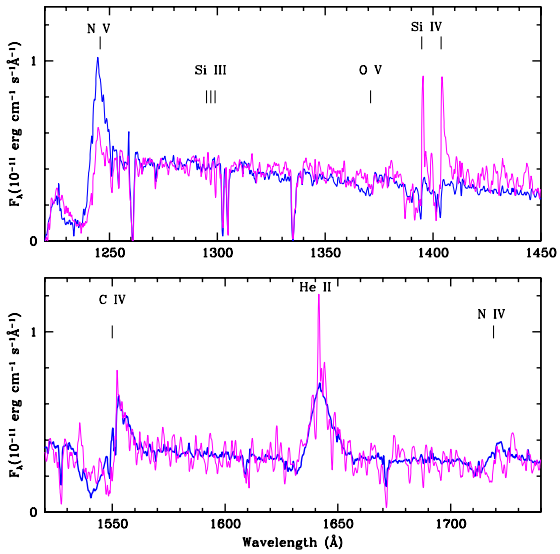


Fig. 11. Average spectrum of HD 5980 in 1979 (dark) and spectrum swp53226 of 1994 (light) illustrating that the underlying C IV and He II emission lines in 1994 are very similar to those in 1979, thus implying their origin in star B. The fluxes are not corrected for reddening, and the 1979 spectrum at $\lambda > 1500$ Å was shifted vertically by $1.\times10^{-12}$ ergs cm$^{-2}$ s$^{-1}$ Å$^{-1}$ to align the continuum level with that of the 1994 spectrum.

N IV] 1486 Å emission, however, is not saturated, and it reaches maximum in 1995a. Values of N IV] 1486 Å for different orbital phases display only a small scatter, indicating that this line is not significantly affected by either geometrical or atmospheric eclipses. This is consistent with two factors: (1) N IV] 1486 Å is produced through a semi-forbidden transition, and thus, the absorption cross-section is very small compared with that of lines such as He II 1640 Å or the resonance lines; (2) it is formed in a very extended wind region.

Plotted on the same scale as N IV] 1486 Å the N V 1240 Å blend (top panel of Fig. 9) displays a huge scatter. However, upon closer inspection, one finds that the large scatter is associated with orbital-phase variability. N V 1240 Å displays systematic trends for the different orbital phase intervals, as illustrated by least-squares fits (dotted lines; eruption data excluded): for $\phi \sim 0.36$ (triangles; star B in front), there is nearly no epoch-dependence; for $\phi \sim 0.0$ (open squares) there is an increasing trend; and data at phases other than near eclipses display a slightly decreasing trend with time.

### 3.3. *Star B: the WR Star?*

Some of the earliest investigations of HD 5980 report a broad and variable emission line from He II 4686 which undergoes changes in FWHM on orbital timescales (Feast, Thackeray, & Wesselink 1960; Breysacher & Westerlund 1978; data of 1975-77; BMN82). The line is narrowest at conjunctions, a characteristic that is still observed in recent spectra. This variability, together with the fact that the RV variations curve of He II 4686 does not follow the orbital motion of star B (BMN82), prompted Moffat et al. (1998) to suggest that a significant fraction of the HD 5980 emission line spectrum may arise in the wind-wind collision (wwc) region between the two stars. This raises the possibility that star B is not really a WR star, but an early O-type star with a significant stellar wind which, when colliding with the wind of star A, leads to a rich emission-line spectrum. An additional caveat to the WNE classification for star B is the 15 $R_\odot$ radius that was derived by BP91 from the eclipse light curve, because the radii of *bona fide* WNE stars are expected to be significantly smaller. There are, however, four lines of evidence supporting the WNE nature of star B.

The original hypothesis that star B is a WR star of the WNE type is based on the long duration of the eclipse when star B is "in front" of star A, which

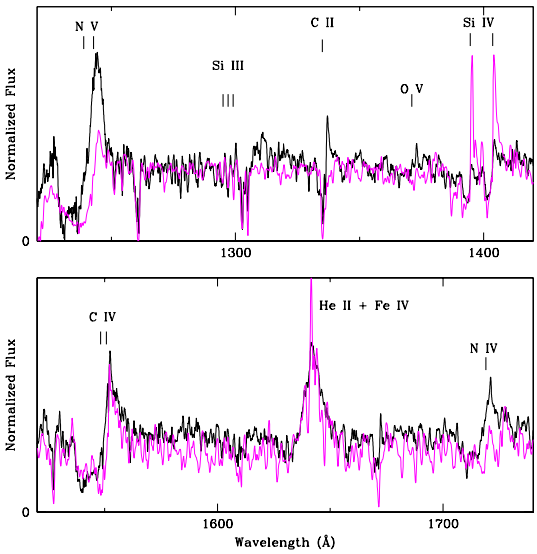


Fig. 12. Comparison between the normalized swp53226 spectrum illustrated in the previous figure (light) and a synthetic spectrum (dark) constructed with normalized and scaled WN4-type (swp6999×0.29), B1Ia$^+$ (swp1822×0.41), and O4If (swp06967×0.30) spectra. The synthetic triple-star system lines of Si III, C IV, and He II are comparable with those observed in swp53226. The difference in N V 1240 and N IV 1718 could be due to wind eclipse effects which in He II may be masked by Fe IV emission.

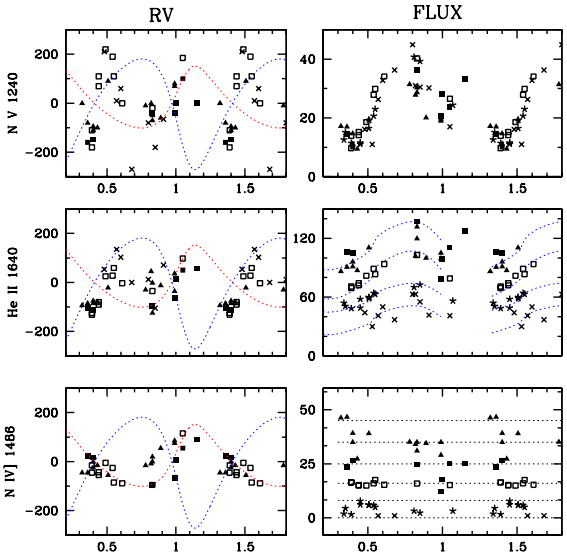


Fig. 13. Phase-dependent variations of the N V 1240, He II 1640, and N IV] 1486 Å emission components. Different symbols represent: 1979/81 (crosses), 1986 (stars), 1989/91 (open squares), 1995 (filled triangles), 1999/2002 (filled squares). RV curves on the left panels are from orbital solution of Niemela et al. (1997); dashed curves on the right panels show trends for different epochs.

implies the presence of an extended semi-opaque region surrounding star B (BP80; BP91). This region would also be responsible for the broad line-emission of He and N.

The second line of evidence is that provided by Niemela's (1988) $\sim$ 500 km s$^{-1}$ amplitude RV variations of N IV 4058, and an orbital phase behavior consistent with its origin in star B. These data were obtained in 1978-1981. In the UV spectrum, N IV] 1486 (which we associate with star A) was barely detectable in 1981, but was clearly present in the spectrum by 1986. During 1981-1983 the RV variations in N IV 4058 were no longer detected (Barbá & Niemela 1995). Thus, the explanation for the behavior of N IV 4058 is that in the earlier observations only star B was contributing towards this emission, while in the later observations both stars contributed, erasing the RV variations. This argument corroborates the presence of N IV 4058 emission in star B but does not unambiguously lead to the conclusion that the line is formed in a dense stellar wind; i.e., it could be formed in the wwc shock region that lies very close to star B's surface.

A third line of evidence is the RV variations curve of He II 4686 given by BMN82. The data that were obtained by these authors between 1975-1979 are plotted in Figure 10 (open squares) and compared with the predicted RV curves of star A and star B according to the Niemela et al. orbital solution (dashes). These curves are shifted by +150 km s$^{-1}$ to correct for the relative motion of the SMC. Clearly, He II 4686 follows the orbital motion of star B for at least a portion of the orbital cycle ($\phi \sim 0.5$–$0.9$); i.e., from near apastron to just before the eclipse of star B by star A. This argues in favor of star B as the origin of the He II emission, but the discrepancy between predicted and observed RV's at orbital phases $\phi \sim 0.1$–$0.4$ remains to be explained. This behavior is not consistent with a simple superposition of two He II emission lines, one from each star, as suggested by BMN82. This is illustrated by the curve plotted with triangles in Fig. 10. The data points were produced by combining individual line profiles that were shifted at each orbital phase according to the

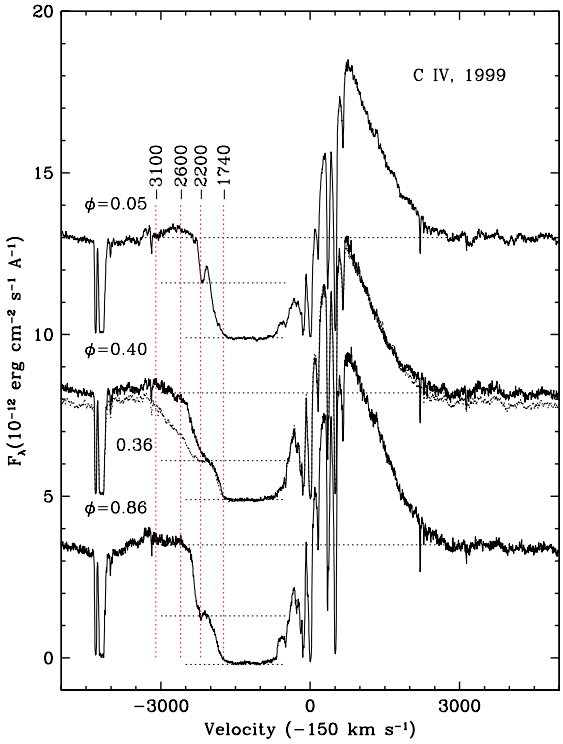


Fig. 14. Line profiles of C IV 1548,1550 Å in 1999 as a function of velocity referred to the $\lambda$1548 line, corrected for SMC motion. Profiles at $\phi = 0.36$ (dotted tracing) and $\phi = 0.40$ were given the same shift, while the $\phi = 0.05$ profile was shifted by twice that amount. Vertical lines mark the location of $v_{black} = -1740$ km s$^{-1}$, $v_{shoulder} \sim -2200$ km s$^{-1}$, and $v_{edge} = -2600$ and $-3100$ km s$^{-1}$.

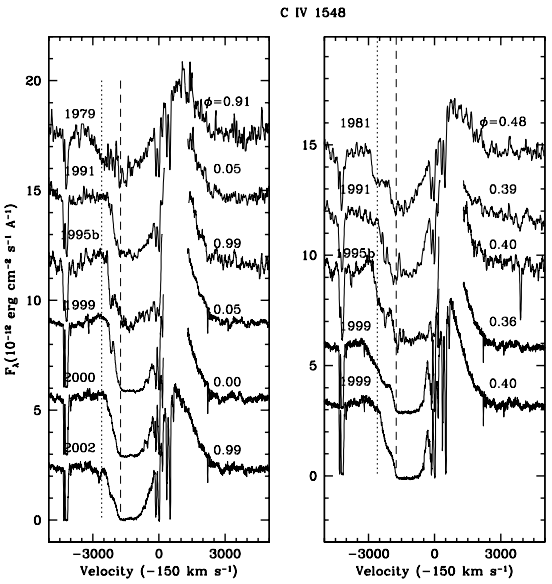


Fig. 15. Line profiles of C IV 1548,1550 Å at orbital phases near $\phi = 0$ (star A "in front", left panel) and $\phi = 0.36$ (star B "in front") for different epochs.

RV curves of star A and star B, and measuring the centroid of the resultant line profile. The template that was used for the "intrinsic" line profile of each star was HD 5980's own He II 4686 in 1973,[4] from observations obtained by N. Walborn, who kindly authorized their use for this purpose. Thus, the assumption that both stars A and B have strong overlapping He II emission leads to a small-amplitude sinusoidal RV curve with extrema at the same phase as the extrema of star B's RV curve, contrary to what is observed. Since the discrepant points in the observed RV curve correspond to the phase interval that occurs immediately after periastron passage, it is tempting to speculate that strong tidal interactions as well as other proximity effects at periastron may play a role in modifying the distribution of line-emitting gas, erasing the contribution from star B's orbital motion.

The fourth line of evidence for the WR nature of star B is presented in Figure 11, where the average UV spectrum of HD 5980 in 1979 is compared with its spectrum swp53226, obtained in 1994 at $\phi$=0.43 (star B "in front" of star A). Although the spectrum is still dominated by narrow emissions from the eruption, two underlying broad lines at C IV and He II prevail. Their profiles closely resemble the corresponding line profiles observed in 1979. It is difficult to devise a scenario in which the He II line appears to recover the profile it had in 1979 unless it is either (a) formed in star B ; or (b) formed in an equatorial wind of star A, in which case star A would have to have been responsible for the He II emission all along, which is contradicted by the second line of evidence above.

To address the question of whether the spectral lines that are present in swp53226 are consistent with the combined (star A+star B+star C) spectrum for this epoch, Figure 12 (dark tracing) illustrates a synthetic spectrum, constructed with IUE data of HD 190603 (B1.5Ia$^+$; Galactic), HD 187282=WR128 (WN4; Galactic) and HD 269698 (O4I; in the LMC). These spectra were each normalized to the continuum level and then combined after assigning different weights to each one, according to the BP91 luminosity ratios. Al-

[4]This is a somewhat flawed assumption since this profile may contain contributions from both stars. However, the actual shape of the template is not a determining factor for the variations of the centroid of the combined profile, so the conclusion is not affected.

though the BP91 values were derived from the visual light curve and may not be applicable to the UV wavelength region, we have at this time no basis for adopting any other luminosity ratio. The He II line is contributed to the synthetic spectrum almost entirely by the WN4 star. The synthetic spectrum reproduces well the broad C IV and He II profiles in spectrum swp53226 of HD 5980, thus leading to the conclusion that the primary contribution to He II and C IV in 1979/81 arises in star B. These line profiles are consistent with a WN4 type star. The strength of the N V 1240 and N IV 1718 emission lines is significantly weaker in HD 5980 than in the synthetic spectrum which, as will be argued below, may be caused by the wind eclipse of star A by star B 's wind. The wind eclipse should also affect the intensity of He II and C IV. Although the observed He II and C IV emissions are slightly weaker than the synthetic ones, it is difficult to evaluate the magnitude of the effect due to the superposition of the narrow eruption emission lines.

In conclusion, four lines of evidence support the presence of an extended, emission line-forming, region associated with star B and the emissions have profiles and degrees of ionization that are consistent with a WN4 spectral type. However, a determination of the N-abundance through a NLTE model fit to the pre-1980's spectrum is required before this conclusion may be unquestionably established.

## 4. ORBITAL-PHASE DEPENDENT VARIATIONS

### 4.1. *UV Line Fluxes and Centroids*

The measured centroids and fluxes of N V 1240, He II 1640, and N IV] 1486 Å emission components are listed in Table 2 and plotted, as a function of orbital phase in Fig. 13. Different symbols represent the observation epochs: 1979/81 (crosses), 1986 (stars), 1989/91 (open squares), 1995 (filled triangles), 1999/2002 (filled squares). RV's (in km $s^{-1}$) are with respect to the average value of each line. The fluxes are the energy contained between the continuum level and the emission line, uncorrected for reddening, and are given in units of $10^{-12}$ ergs $cm^{-2}$ $s^{-1}$. The RV curves are taken from the Niemela et al. (1997) orbital solution.

The N IV] data clearly follow star A's RV curve, showing that this line is formed mostly in star A. Its flux levels increase systematically with epoch, but do not undergo significant phase-dependent variability despite the strong profile variability that this line presents. The He II and N V lines tend to follow the RV curve of star A during the phase interval in which this star is "in front", while they are more similar to the RV curve of star B when it is "in front". Extreme caution is necessary, however, when interpreting the RV variations because the distortion of the line profiles by interaction effects within the binary lead to significant departures from the predicted motion due to orbital motion alone. The phase-dependence of these two line fluxes is remarkable. N V has, surprisingly, no epoch-dependence but shows a very strong phase dependence; the behavior of He II is mixed, with both an epoch dependence (similar to that of N IV] 1486 Å) and phase dependence (similar to that of N V). This is illustrated with the dashed curve that is shifted along the vertical scale to coincide with each data set.

The phase-dependent flux variability is most naturally explained with wind eclipses. N V has a large transition probability, and as both stars possess stellar winds, the eclipse by each wind of the companion's continuum produces strong absorption at line frequencies; the stronger eclipse occurring at $\phi$=0.36 because of the larger size and brightness of star A's continuum-emitting region. No such effect is observed in N IV] 1486 Å because it is a semi-forbidden line, and the transition probability is significantly smaller, and also because it is formed only in the wind of star A. Wind eclipses have already been shown to produce significant UV line-profile variability in HD 5980 and several other WR+O binary systems (Willis et al. 1979; Koenigsberger & Auer 1985; Auer & Koenigsberger 1994). The possible presence of a wind eclipse at $\phi \sim 0.0$ in HD 5980 was also noted by Moffat et al. (1989), supporting the idea of a relatively dense wind in star A in 1986. The effect of the wind eclipses on the line profiles is most likely the dominant factor causing the complicated RV variations curves of these lines, unlike N IV] 1486 Å which is relatively less affected by the wind eclipses.

### 4.2. *Characteristic Wind Velocities*

The P Cygni absorption lines provide information on the maximum bulk wind speed ($v_\infty$) along the line of sight to the continuum emitting region of the star. Lines arising from resonance transitions are generally saturated and have a flat portion in the absorption trough, the maximum extent of which ($v_{black}$), provides the most reliable measure of $v_\infty$ (see e.g., Prinja, Barlow, & Howarth 1990). In the case of single stars, it is relatively straightforward to determine $v_{black}$. In a multiple system, however, although each star contributes to this absorption, $v_{black}$ corresponds only to the slowest wind in the

TABLE 2

FLUXES AND RADIAL VELOCITIES

| | | N V 1240.83 | | He II 1640.47 | | N IV] 1486.50 | |
|---|---|---|---|---|---|---|---|
| Spec. | $\phi$ | RV[a] | Flux[b] | RV[a] | Flux[b] | RV[a] | Flux[b] |
| 1598[c] | 0.53 | 1600: | 12: | ··· | 30 | ··· | ··· |
| 4277 | 0.57 | 1110 | 26.3 | 360 | 41.0 | 390 | 1 |
| 4345 | 0.91 | 1035 | 30.2 | 296 | 41.7 | np | np |
| 4958 | 0.68 | 830 | 36.3 | 225 | 36.9 | 280: | 1 |
| 11175 | 0.48 | 1310 | 16.1 | 278 | 44.1 | 420: | np |
| 11190 | 0.60 | 1160 | 32.8 | 328 | 50.0 | np | np |
| 14112[c] | 0.82 | ··· | 31 | ··· | 63 | np | np |
| 14166[c] | 0.05 | ··· | 17 | ··· | 41 | np | np |
| 15072 | 0.80 | 1020 | 44.9 | 237 | 62.8 | np: | np |
| 15080 | 0.85 | 920 | 30.5 | 120 | 55.1 | np | np |
| 37759 | 0.39 | 990 | 13.9 | 93 | 70.8 | 80 | 16.4 |
| 37768 | 0.44 | 1210 | 15.2 | 145 | 72.0 | 70 | 15.2 |
| 37781 | 0.55 | 1210 | 29.9 | 284 | 83.4 | 40 | 17.5 |
| 37788 | 0.61 | 1100 | 34.1 | 222 | 93.8 | 37 | 15.3 |
| 42446 | 0.83 | 1080 | 40.2 | 190 | 103.0 | 30 | 15.9 |
| 42470 | 0.05 | 1285 | 26.5 | 323 | 79.0 | 240 | 15.2 |
| 42694 | 0.39 | 920 | 9.7 | 100 | 69.4 | 110 | 16.4 |
| 42702 | 0.44 | 1170 | 14.2 | 134 | 74.2 | 82 | 15.0 |
| 42711 | 0.49 | 1320 | 18.6 | 250 | 81.8 | 120 | 14.9 |
| 42721 | 0.54 | 1290 | 27.9 | 253 | 88.8 | 99 | 16.0 |
| 52888 | 0.51 | np | 1.1 | ··· | ··· | 340 | 11.2 |
| 53036 | 0.39 | np | np | 141: | 32: | 130 | 16.8 |
| 53129 | 0.86 | 500: | 3.5 | 460: | 19: | 300 | 10.4 |
| 53185 | 0.17 | 1170 | 4.4 | 465: | 14: | 160 | 12.0 |
| 53216 | 0.38 | 1630 | np | 342: | 48: | 150 | 26.0 |
| 53226 | 0.43 | 1170 | 4.7 | 323: | 55: | 60 | 24.8 |
| 54064 | 0.89 | 1040 | 20.1 | 213 | 100 | 180 | 34.5 |
| 54490 | 0.32 | 1100 | 17.2 | 131 | 86.4 | 80 | 46.3 |
| 54671 | 0.36 | 1020 | 17.0 | 140 | 90.7 | 80 | 46.6 |
| 54727 | 0.82 | 1100 | 27.8 | 270 | 102.0 | 117 | 34.0 |
| 55315 | 0.78 | 1090 | 31.4 | 195 | 155.5 | 110 | 35.1 |
| 55380 | 0.40 | 990 | 11.2 | 140 | 96.1 | 100 | 39.2 |
| 55394 | 0.50 | 1190 | 19.5 | 203 | 110.4 | 70 | 39.0 |
| 55932 | 0.83 | 1050 | 28.7 | 223 | 131.7 | 145 | 35.0 |
| 55955 | 0.99 | 1180 | 19.0 | 261 | 99.3 | 210 | 35.0 |
| 56017 | 0.40 | 1005 | 14.7 | 150 | 91.2 | 125 | 35.0 |
| 56188 | 0.83 | 1030 | 30.3 | 100 | 119.8 | 125 | 31.0 |
| 56205 | 0.99 | 1170 | 19.7 | 189 | 105.0 | 200 | 29.0 |
| 56223 | 0.43 | 1000 | 9.5 | 145 | 87.4 | 110 | 27.3 |
| o1070 | 0.86 | 1060 | 36.4 | 128 | 136.8 | 30 | 24.9 |
| o3070 | 0.05 | 1200 | 23.7 | 275 | 111.1 | 180 | 25.0 |
| o4070 | 0.15 | 1100 | 33.1 | 283 | 127.4 | 216 | 25.0 |
| o5070 | 0.36 | 940 | 14.5 | 120 | 105.6 | 150 | 23.6 |
| o6070 | 0.40 | 950 | 10.1 | 112 | 105.0 | 140 | 26.4 |
| o2070 | 0.01 | 1100 | 28.2 | 239 | 98.7 | 130 | 17.9 |
| o1020 | 0.99 | 1060 | 20.7 | 160 | 78.8 | 60 | 12.2 |

[a]RVs are the centroid of the line, in km $s^{-1}$, with respect to the wavelength listed in the table head (no correction for SMC motion); np indicates line not present.

[b]Integrated fluxes ($10^{-12}$ erg $cm^{-2}$ $s^{-1}$), not corrected for reddening, obtained by fitting Gaussian or Lorentzian profiles; peak intensities of N V and He II saturated the detector in all observations after 1981, and thus these values are lower limits.

[c]Low dispersion spectrum.

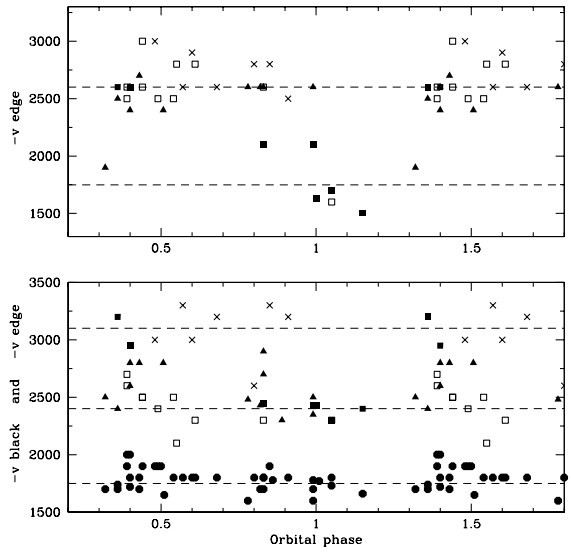


Fig. 16. Orbital phase dependence of $v_{edge}$ for He II 1640 Å (top) and C IV 1548 Å (bottom) plotted with different symbols corresponding to the epoch of observation: 1979/81 (crosses), 1989/91 (open squares), 1995 (triangles), and 1999/2002 (filled squares). Filled circles represent $v_{black}$ for C IV 1548 Å at all epochs. The horizontal lines mark some of the characteristic velocities.

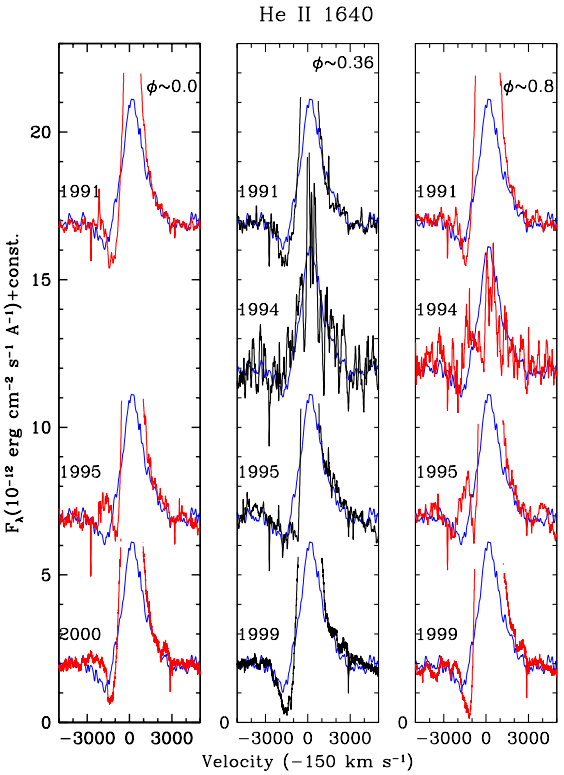


Fig. 17. Line profiles of He II 1640 Å at orbital phases near the eclipses (0.0 and 0.36) and an elongation (0.83) between 1991 and 1999 (dark lines), compared with the line profile in 1979 (swp4277, light tracing).

system. The other winds' values of $v_{black}$ are not at zero flux levels, but may be visible as a "shoulder" or "step" ($v_{shoulder}$) in the absorption line profile (Georgiev & Koenigsberger 2004b). The maximum extent of the absorption, $v_{edge}$, defined as the location where the absorption line profile intersects the continuum, generally yields velocities that are $\sim 25\%$ larger than $v_{black}$, and is believed to reflect "turbulent" motions within the supersonically expanding wind.

Values of $v_{edge}$ measured on 1979–1995 IUE data (Koenigsberger et al. 1998a) suggested a trend to slower speeds (from $\sim -3000$ km s$^{-1}$ to $-2100$ km s$^{-1}$) prior to the eruption (1979–1991 data). At the time of the eruption, significantly slower ($\sim -400$ to $-900$ km s$^{-1}$) edge velocities were present. In the months following the eruption, three sets of characteristic velocities were identified: a) a shoulder at $-1100$ to $-1300$ km s$^{-1}$, b) an edge at $-2100$ to $-2600$ km s$^{-1}$, and c) $v_{black}$ at $-1700$ km s$^{-1}$. Because of the apparent decreasing trend in edge speeds between 1979 and 1991, Koenigsberger et al. (1998a) concluded that the fast ($\sim -3000$ km s$^{-1}$) wind in 1979 belonged to star A. In this section this conclusion is re-examined in the light of the more recent *HST* spectroscopic data. These data imply that currently the most likely wind speeds for stars A and B are, respectively, in the ranges $v_\infty$(A) $\sim -1700$ to $-2200$ km s$^{-1}$ and $v_\infty$(B) $\sim -2600$ to $-3100$ km s$^{-1}$, suggesting that the fast edge speeds of 1979/81 are most likely associated also with star B. However, the actual origin of the $\sim -3000$ km s$^{-1}$ edges in 1979/81 cannot be unambiguously established at this time.

A sample of the C IV P Cygni line profiles of HD 5980 is shown in Figure 14, plotted on a velocity scale (referred to the $\lambda$ 1548 component), corrected for the SMC motion (assumed to be +150 km s$^{-1}$). The horizontal dashes mark the flux levels of $v_{black}$, $v_{shoulder}$, and the adopted continuum level. Tables 3 and 4 list the values of the velocities measured on each of the individual spectra, for C IV 1548 and He II 1640 Å, respectively. The orbital phase-dependent variability consists primarily of changes in the extent of $v_{edge}$, with a systematic trend for a more extended $v_{edge}$ around $\phi = 0.36$, when star B is "in front". This trend is present at all epochs after 1981, illustrated in Figure 15,

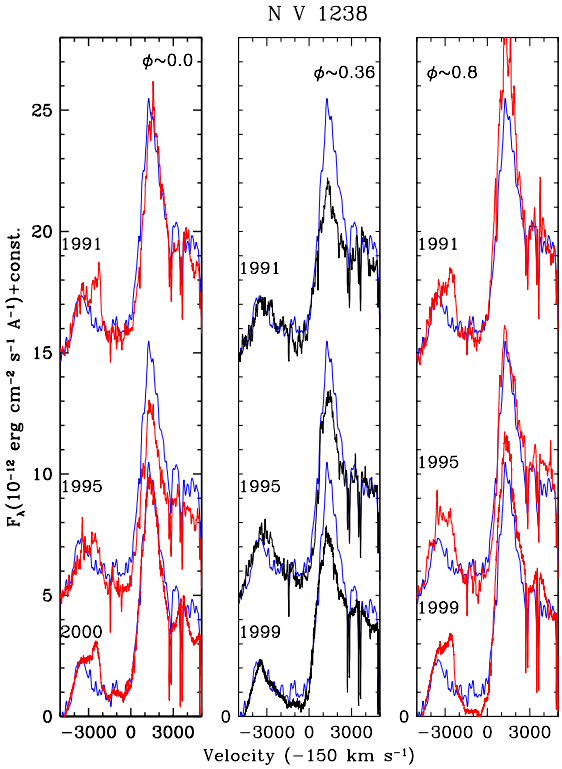


Fig. 18. Line profiles of N V 1238 Å at orbital phases near the eclipses (0.0 and 0.36) and an elongation (0.83) between 1991 and 1999 (dark lines), compared with the line profile in 1979 (swp4277, light tracing). No relative shifts in the vertical scale were applied except for the fixed displacement between different epochs.

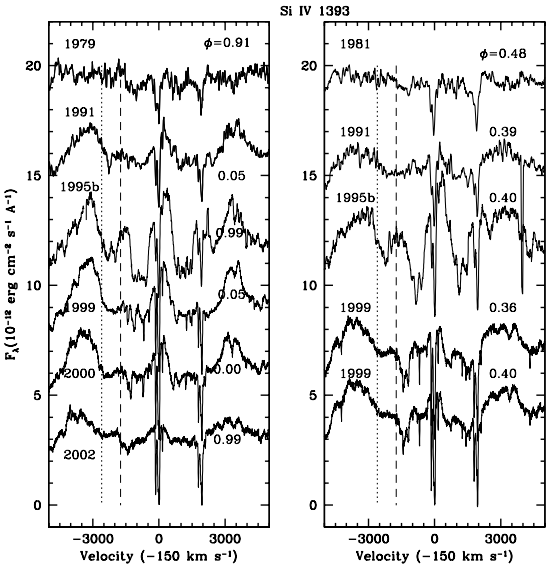


Fig. 19. Line profiles of Si IV 1393,1402 Å at orbital phases near $\phi = 0$ (star A "in front", left panel) and $\phi = 0.36$ (star B "in front"). Same spectra as in Figs. 17 and 18.

where the C IV line near the two orbital phases, $\phi \sim 0.0$ and 0.36 is shown. In Figure 16 (bottom panel), $v_{edge}$ (C IV) is plotted as a function of orbital phase. The different symbols correspond to different epochs of observations. Unfortunately, high resolution data are available for epoch 1979/81 (crosses) only in the phase interval 0.5−0.9. A marked difference between 1979/81 and 1989/91 (open squares) is evident with the former epoch showing $V_{edge}$ (C IV, 1979/81) $\sim -3200$ km s$^{-1}$ while $v_{edge}$ (C IV, 1989/91) $\sim -2400$ km s$^{-1}$. Near $\phi = 0.4$, the data for 3 epochs indicate $v_{edge} \sim -2700\pm200$ km s$^{-1}$, while at $\phi \sim 0.9-1.3$, $v_{edge} \sim -2400$ km s$^{-1}$ for 1989-2001.

In general, the measurement uncertainties are $\sim 150$ km s$^{-1}$ for $v_{edge}$ in C IV, while the uncertainties are larger (up to $\sim 300$ km s$^{-1}$) for $v_{shoulder}$ and the velocities of He II, depending on the quality of the data.

Variability with orbital phase of $v_{black}$ is not detected, as illustrated with the black circles in the bottom panel of Fig. 16. Its mean value is $-1790$ km s$^{-1}$, although there is a tendency for slighly larger values ($-1850$ km s$^{-1}$) prior to the eruption (1979–1991).

From the bottom panel of Fig. 16, one conclusion that may be reached is that during the epochs 1989-2001, the winds of the three stars have $v_\infty \sim -1700$ (star C), $-2600$ (star B), and $-2400$ (star A; excluding the eruptive phase) km s$^{-1}$. However, the very fast edges ($\sim -3100$ km s$^{-1}$) observed in 1979/81 are perplexing. Figures 17 and 18 illustrate, respectively, the He II 1640 Å and N V 1240 P Cygni profiles at different epochs, for three different orbital phases, $\phi = 0.0$ (star A in front), 0.36 (star B in front) and 0.8. The light tracing superposed on each profile corresponds to spectrum swp4277, obtained in 1979. The P Cygni absorption components for all epochs at $\phi \sim 0.36$ are similar to those observed in 1979, suggesting that the fast wind arises in star B. If this is the case, then an explanation is needed to account for the slower $v_{edge}$ observed in subsequent epochs at all phases except during 1999, $\phi = 0.36$, since star B is not supposed to have changed its wind structure.

Unlike C IV, He II is not a resonance line and it does not produce a saturated (i.e., $v_{black}$) absorp-

TABLE 3

C IV 1548 Å VELOCITIES

| Spectrum | HJD −2400000 | Phase | Velocities[a] $V_{black}$ | $V_{shoulder}$ | $V_{edge}$ | Comments |
|---|---|---|---|---|---|---|
| **1979/81** | | | | | | |
| 4277 | 43921.1 | 0.57 | −1800 | −2500 | −3300 | |
| 4345 | 43928.6 | 0.91 | −1800 | −2600 | −3200 | |
| 4958 | 43981.0 | 0.68 | −1800 | −2700 | −3200 | |
| 11175 | 44632.3 | 0.48 | −1900 | −2600 | −3000 | |
| 11190 | 44634.6 | 0.60 | −1800: | ··· | −3000 | |
| 15072 | 44869.5 | 0.80 | −1800 | −2400 | −2600 | |
| 15080 | 44870.5 | 0.85 | −1900 | −2500 | −3300 | |
| **1989/91** | | | | | | |
| 37759 | 47867.2 | 0.39 | −1900 | −2300 | −2700 | |
| 37768 | 47868.2 | 0.44 | ··· | ··· | −2500 | |
| 37781 | 47870.2 | 0.55 | ··· | ··· | −2100 | |
| 37788 | 47871.4 | 0.61 | −1800 | −2000 | −2300 | |
| 42446 | 48511.5 | 0.83 | −1800 | −2100 | −2300 | |
| 42470 | 48515.6 | 0.05 | −1800 | −2000 | −2300 | |
| 42694 | 48541.4 | 0.39 | −2000 | −2300 | −2600 | |
| 42702 | 48542.4 | 0.44 | −1900 | −2300 | −2500 | |
| 42711 | 48543.4 | 0.49 | −1900 | −2300 | −2400 | |
| 42721 | 48544.4 | 0.54 | −1800 | −2200 | −2500 | |
| **1994** | | | | | | |
| 52888 | 49680.5 | 0.51 | −1650: | ··· | −1770 | |
| 53036 | 49697.5 | 0.39 | ··· | ··· | −1740 | |
| 53129 | 49706.5 | 0.86 | ··· | ··· | ··· | |
| 53185 | 49712.4 | 0.17 | ··· | ··· | ··· | |
| 53216 | 49716.5 | 0.38 | ··· | ··· | ··· | |
| 53226 | 49717.5 | 0.43 | −1700: | −400: | −2300: | em on blue edge? |
| **1995a** | | | | | | |
| 54064 | 49784.1 | 0.89 | ··· | −2000 | −2300 | em on blue edge |
| 54490 | 49831.0 | 0.32 | −1700 | ··· | −2500 | em on blue edge |
| 54671 | 49851.0 | 0.36 | −1700 | −2100 | −2400 | em on blue edge |
| 54727 | 49859.9 | 0.82 | −1700 | −2300 | −2400 | em on blue edge |
| 55315 | 49916.8 | 0.78 | −1600 | −2100 | −2500 | em on blue edge |
| 55380 | 49928.8 | 0.40 | −2000 | −2200 | −2600 | |
| 55394 | 49930.8 | 0.50 | −1900 | ··· | −2800 | |
| **1995b** | | | | | | |
| 55932 | 49975.6 | 0.83 | −1700 | −2400 | −2700 | em on blue edge? |
| 55955 | 49978.7 | 0.99 | −1700 | −2300 | −2500 | |
| 56017 | 49986.6 | 0.40 | −1800 | −2300 | −2800 | |
| 56188 | 50033.5 | 0.83 | −1800: | −2300 | −2900 | |
| 56205 | 50036.4 | 0.99 | −1600 | −2200 | −2300 | |
| 56223 | 50045.2 | 0.43 | −1800 | −2200 | −2800 | |
| **1999** | | | | | | |
| o1070 | 51304.8 | 0.86 | −1780 | −2250 | −2440 | |
| o3070 | 51308.9 | 0.05 | −1730 | −2170 | −2300 | |
| o4070 | 51310.8 | 0.15 | −1660 | −2170 | −2440 | |
| o5070 | 51314.9 | 0.36 | −1740 | −2260 | −3230 | |
| o6070 | 51315.8 | 0.40 | −1720 | −2170 | −2960 | |
| **2000** | | | | | | |
| o2070 | 51655.1 | 0.01 | −1770 | −2260 | −2420 | |
| **2002** | | | | | | |
| o1020 | 52386.6 | 0.99 | −1780 | −2230 | −2420 | DAC at −2770? |

[a]Velocities corrected for SMC motion (+150 km s$^{-1}$); uncertainty in IUE data is in general ±100 km s$^{-1}$.

TABLE 4

He II 1640 Å VELOCITIES

| Spectrum | Phase | He II velocity[a] | | | FWHM | Comments[b] |
|---|---|---|---|---|---|---|
| | | $v_{shoulder}$[c] | $v_{edge}$ | $v_{red}$[c] | Emission | |
| **1979/81** | | | | | | |
| 4277 | 0.57 | ··· | −2600 | 3000 | 2150 | |
| 4345 | 0.91 | ··· | −2500 | 3100 | 2320 | |
| 4958 | 0.68 | −1600 | −2600 | 2700 | 2350 | |
| 11175 | 0.48 | −1800 | −3000 | 2600 | 2090 | |
| 11190 | 0.60 | ··· | −2900 | 2600 | 1870 | |
| 15072 | 0.80 | −2000 | −2800 | 2900 | 2330 | |
| 15080 | 0.85 | ··· | −2800 | 3000 | 2590 | |
| **1989/91** | | | | | | |
| 37759 | 0.39 | −2000 | −2500: | 2900 | 1360 | |
| 37768 | 0.44 | −1700 | −3000 | 3200 | 1620 | |
| 37781 | 0.55 | −1800 | −2800 | 2900 | 1520 | |
| 37788 | 0.61 | −1800 | −2800 | 3300 | 1620 | |
| 42446 | 0.83 | −1700 | −2600: | 3000: | 1950 | |
| 42470 | 0.05 | −1300: | −1600 | 2900 | 1450 | |
| 42694 | 0.39 | −2100: | −2600 | 2900 | 1310 | |
| 42702 | 0.44 | ··· | −2600 | 3000 | 1430 | |
| 42711 | 0.49 | −1600 | −2500 | 2900 | 1380 | |
| 42721 | 0.54 | ··· | −2500: | 2900 | 1440 | |
| **1994** | | | | | | |
| 52888 | 0.51 | ··· | −500 | ··· | 2600:: | |
| 53036 | 0.39 | ··· | −400 | ··· | 1900:: | |
| 53129 | 0.86 | ··· | −400 | ··· | ··· | |
| 53185 | 0.17 | ··· | −400 | ··· | ··· | |
| 53216 | 0.38 | ··· | −400 | ··· | 2000: | |
| 53226 | 0.43 | ··· | −400 | ··· | 2000: | |
| **1995a** | | | | | | |
| 54064 | 0.89 | −1200 | −2600:: | 2500: | 1300 | |
| 54490 | 0.32 | ··· | −1900 | 2800: | 1100 | DAC at −800 |
| 54671 | 0.36 | −1100 | −2500: | 3300: | 1200 | DAC at −800 |
| 54727 | 0.82 | −1100 | −2600: | 3300: | 1500 | |
| 55315 | 0.78 | −1100 | −2600: | 3300: | 1590 | |
| 55380 | 0.40 | −1800 | −2400 | 3300: | 1190 | |
| 55394 | 0.50 | −1000: | −2400 | 2800 | 1450 | |
| **1995b** | | | | | | |
| 55932 | 0.83 | −1100 | −2600 | 3200 | 1570 | |
| 55955 | 0.99 | −1200 | −2600: | 3000 | 1500 | |
| 56017 | 0.40 | −1800 | −2600 | 2900 | 1380 | DAC at −1000 |
| 56188 | 0.83 | −1400: | −2500:: | 2900 | 1890 | |
| 56205 | 0.99 | −1400 | em | 2900 | 1590 | |
| 56223 | 0.43 | −1300 | −2600 | 2700 | 1150 | |
| **1999** | ··· | | | | | |
| o1070 | 0.86 | −1700 | −2100 | 3100 | 1760 | DAC at −1300? |
| o3070 | 0.05 | −1300 | −1700 | 2900 | 1180 | |
| o4070 | 0.15 | −1300 | −1500 | 3900:: | 1550 | DACs at −1300 and −900? |
| o5070 | 0.36 | −1800 | −2600 | 3900: | 1380 | v.wk. DAC at −1300 |
| o6070 | 0.40 | −1700 | −2600 | 3600 | 1200 | v.wk. DAC at −1300 |
| **2000** | | | | | | |
| o2070 | 0.01 | ··· | −1630 | 2900 | 1300 | |
| **2002** | | | | | | |
| o1020 | 0.99 | ··· | −2100 | 2900 | 1400 | |

[a] Velocities corrected for SMC motion (+150 km s$^{-1}$); DAC is discrete absorption components.
[b] "em" signifies emission.
[c] Here the measurement refers to the end of a deeper portion of absortion.
[d] Uncertainty in red wing placement is ±200 km s$^{-1}$ and in $V_{edge}$ is between ±100 and ±300 km s$^{-1}$, depending on the S/N.

tion. In addition, it is not expected to have a strong contribution from star C. Therefore, the velocities obtained from He II may be associated only with either star A or star B. Table 4 lists $v_{edge}$ (He II) and $v_{shoulder}$ (He II) which provides a measure of the maximum extent of the flat-looking portion of the He II absorption component. Although this latter quantity ($v_{shoulder} \sim -1300$ to $-2000$ km s$^{-1}$) may be associated with the star having the slower wind, it could also be reflecting effects due to wind-wind interactions (i.e., a wwc before $v_\infty$ has been attained). The top panel of Fig. 16 is a plot of $v_{edge}$ (He II) as a function of orbital phase which shows a minimum ($v_{edge} \sim -1700$ km s$^{-1}$) between orbital phases 0.9 and 1.3, approximately. Because we have concluded that both stars A and B possess strong He II 1640 Å emission, the conclusion seems inescapable that the maximum wind speed for the He II forming region in star A is $v_{edge}(\phi = 0) \sim -1700$ km s$^{-1}$, given that at $\phi = 0$ the continuum-forming region of star B should be almost completely eclipsed. In the phase-interval 0.36–0.9, $v_{edge} \sim -2400$ to $-3000$ km s$^{-1}$, consistent with an origin in star B.

The maximum extent towards the red of the He II emission component ($v_{red}$) was measured and is listed in column 5 of Table 4. The He II 1640 Å emission reaches the continuum level at $v_{red} \geq 2600$ km s$^{-1}$ with no significant epoch or orbital phase dependence, except 1994 when this line is apparently veiled by the narrow emission lines from the eruption spectrum[5] The extended red wing is particularly evident during 1995a, when the superposed narrow (Gaussian FWHM $\sim 900$ km s$^{-1}$) emission is very strong, but a comparison between, for example, swp55380 ($\phi = 0.40$) and swp4277 (1979) discloses nearly identical He II red wings within the velocity range $1100-3200$ km s$^{-1}$. This further supports the conclusion that star B emits a very broad He II line.

The last column of Table 4 lists the values of the He II 1640 Å full width at half-maximum intensity (FWHM), measured by fitting a Gaussian to the line profiles. The FWHM is largest in 1979/81, when the flux contained in the line is lowest, and decreases at epochs when the flux is larger. This correlation is a natural result of the fact that the enhanced emission (due to star A) has a narrower line profile which, when superposed on the broader underlying profile, raises the level of "half maximum" to positions on the line profile corresponding primarily to the emission from star A. With respect to the orbital phase-dependence, the general trend for smaller FWHM at eclipses that is observed in optical He II lines persists in the UV.

The evidence pointing towards star B as the origin of $v_{edge} \sim -3100$ km s$^{-1}$ is very strong. The question remains, however, of why the $\sim -3100$ km s$^{-1}$ speeds are not observed at orbital phases other than 0.36 in epochs such as 1989/91, since star B is in full view of the observer at all phases except near $\phi = 0.0$. One possible explanation is that once the wind of star A becomes dominant, the wind-wind collision shock cone wraps around star B and constrains star B's wind, preventing it from attaining $v_\infty$ except on the open end of the shock cone. Another possibility is that the $\sim -3100$ km s$^{-1}$ speeds are due to "turbulent" motions, instead of bulk wind speed, and that the "turbulence" is variable. From the two *HST* spectra at $\phi = 0.36$ and 0.40 illustrated in Fig. 14, a timescale for the variability of $< 1$ day can be established. Note that these two profiles are plotted with no relative vertical shift, and though there is a remarkable change in the extent of $v_{edge}$ and $v_{shoulder}$, the rest of the profile remains constant, suggesting that the difference in wind structure producing the absorption is localized "in front" of the continuum sources, rather than in a more extended region.

Similar changes in the N V 1240 and He II 1640 Å P Cygni absorptions are also present, but absent in Si IV, as shown in Figure 19. Since Si IV 1400 Å is mainly associated with star A, there is little doubt that the rapid change in $v_{edge}$ between $\phi$ =0.36 and 0.40 is associated with star B. But the limited number of UV spectra makes it very difficult to determine whether the effect is due to the wwc shock cone effect or due to variable turbulent motions. It is interesting to note, however, that Villar-Sbaffi et al. (2003) find strong variability in polarization measurements near $\phi$ =0.36, consistent with a large degree of short timescale variability in the wind of star B.

## 5. THE ROLE OF WIND-WIND COLLISIONS

There are at least three interaction effects that produce line-profile variability: (1) physical eclipses in which the emitting region is blocked by the stellar disk of the companion; (2) wind eclipses in which the stellar disk of one star is occulted by the wind of the second star; and (3) wind-wind collisions. As previously shown (Auer & Koenigsberger 1994; Georgiev & Koenigsberger 2004b), wind eclipses can account for a significant amount of the UV line-profile variability in WR+O binary systems in resonance lines and permitted lines arising in transitions between low-lying excited atomic levels. The flux variability

[5]The extraordinary extent of the red emission wings, in general, is attributed to electron scattering.

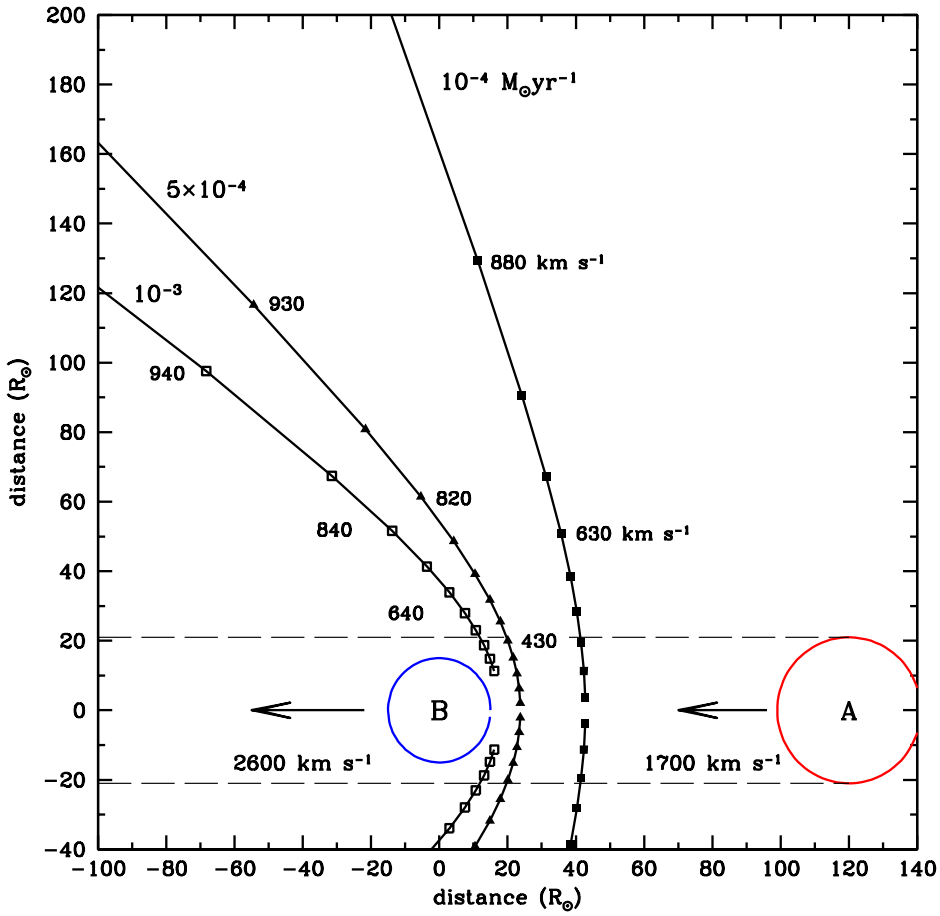


Fig. 20. Shape of the wwc shock cones under the thin shock approximation for three values of star A's mass-loss rate ($\dot{M}_A = 1\times10^{-4}$, $5\times10^{-4}$, and $1\times10^{-3}$ $M_\odot$ yr$^{-1}$), and $\dot{M}_B = 2\times10^{-5}$ $M_\odot$ yr$^{-1}$. The different symbols along the shock cone walls indicate locations for which tangential velocities were computed, some of which are listed. The dashed lines enclose the wind material that is projected onto the continuum-emitting cores of the two stars at $\phi = 0.36$, assuming the observer is on the left side of the figure.

displayed by N V 1240 and He II 1640 Å in HD 5980 (Fig. 13) is consistent with that expected from the wind eclipses. However, the potential effects of wind-wind collisions are difficult to predict, unless the characteristics of the two stellar winds and the wwc shocks are known. Having established the range of velocities in HD 5980 at which star A and star B winds are expanding, a preliminary analysis of the role played by the wwc in producing line-profile variability may be made.

The wind-wind interaction has four potential effects: (a) it breaks the spherical symmetry of the stellar winds (assuming that they are intrinsically spherically symmetric); (b) it may truncate the wind within its accelerating region preventing it from achieving $v_\infty$; (c) the post-shock material that flows along the shock cone walls may produce emission lines that are superposed on the stellar wind lines; (d) portions of the shock cone are expected to be sources of X-ray emission that can modify the ionization structure of the incoming, pre-shock stellar winds. Each one of these effects produces orbital-phase dependent variability, but only the effects (a) and (b) have been incorporated into a model (Georgiev & Koenigsberger 2004b). Some insight may be gained by using the simplest approach pos-

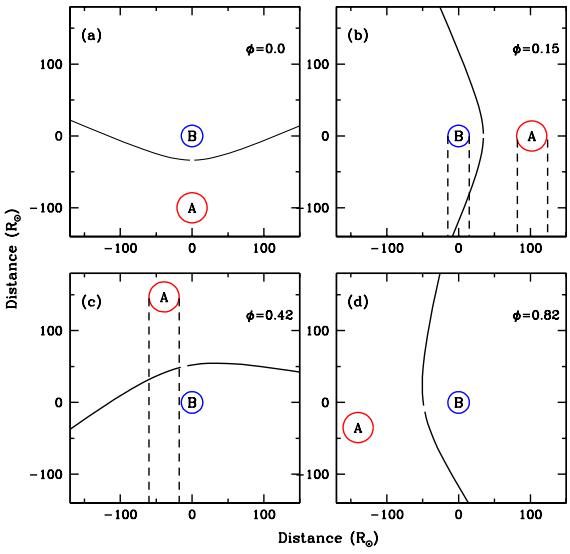


Fig. 21. Geometry of the orbit and wwc region in HD 5980 at different orbital phases. Shaded areas illustrate the columns of wind material projected onto star A's continuum-forming region and in which P Cygni absorption components are produced. Parameters are $\dot{M}_A = 1{\times}10^{-4}\ M_\odot\ \mathrm{yr}^{-1}$, $\dot{M}_B = 2{\times}10^{-5}\ M_\odot\ \mathrm{yr}^{-1}$ $v_\infty(\mathrm{A}) = 2000\ \mathrm{km\ s}^{-1}$, $v_\infty(\mathrm{B}) = 2600\ \mathrm{km\ s}^{-1}$.

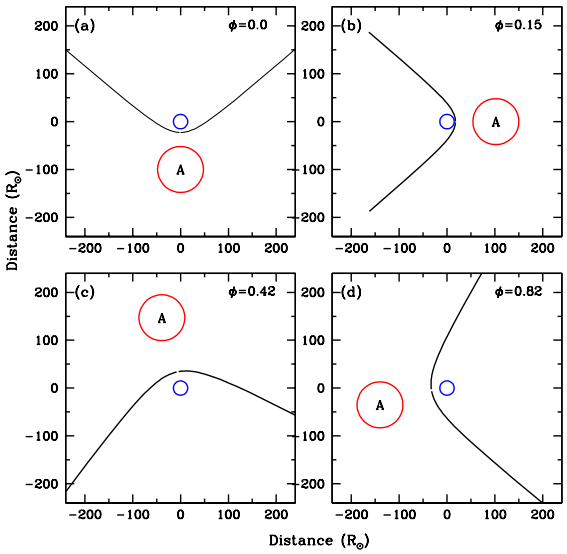


Fig. 22. Representation of the geometry of HD 5980 wwc for $\dot{M}_A = 1{\times}10^{-3}\ M_\odot\ \mathrm{yr}^{-1}$, and $v_\infty(\mathrm{A}) = 600$ km s$^{-1}$, $\dot{M}_B = 2{\times}10^{-5}\ M_\odot\ \mathrm{yr}^{-1}$, and $v_\infty$(B)=2600 km s$^{-1}$, corresponding to December 30, 1994 (swp53226). At $\phi = 0.4$, extinction of star A's continuum by star B's wind is expected to be large.

sible: the two winds are assumed to collide at their terminal speeds, and cooling is efficient enough so that the two shock surfaces that separate the winds lie very close together (i.e., the thin shock approximation). Under these assumptions, the analytic solution of the conservation of energy and momentum equations of Cantó et al. (1996) is valid, and this allows a precise determination of the geometry of the wwc shock surfaces and the tangential flow velocity along these surfaces.

### 5.1. *Geometry of the Wind-Wind Collision Region*

Cantó, Wilkin, & Raga (1996) find simple algebraic expressions for the location $R(\theta)$ of the shock cone walls and the tangential velocity $v_t(\theta)$ of the gas that flows along the shock cone walls after having collided. The angle $\theta$ is measured in the reference frame centered on the star around which the shock cone folds; i.e., the star with the weaker wind. Figure 20 illustrates the configurations for three assumed values of star A's mass-loss rate ($\dot{M}_A = 1 \times 10^{-4}$, $5 \times 10^{-4}$, and $1 \times 10^{-3}\ M_\odot\ \mathrm{yr}^{-1}$), and the slowest deduced wind velocity of star A (1700 km s$^{-1}$) outside of its eruptive event. For star B, we assume that $\dot{M}_B = 2 \times 10^{-5}\ M_\odot\ \mathrm{yr}^{-1}$, typical of WR-star mass loss rates, and $v_\infty(\mathrm{B}) = 2600\ \mathrm{km\ s}^{-1}$. For the three cases, the momentum balance is in favor of star A, and the wwc shock cone wraps around star B. This is even more so if larger $v_\infty$(A) are assumed, an example of which is shown in Figure 21 for $v_\infty(\mathrm{A}) = 2000$ km s$^{-1}$, where the relative location of the wwc shock cone and the two stars is illustrated for different orbital phases. The observer is placed at the bottom of the figure. Other parameters are $R_A = 21\ R_\odot$, $R_B = 15\ R_\odot$, $\dot{M}_A = 1 \times 10^{-4}\ M_\odot\ \mathrm{yr}^{-1}$. Given the eccentricity of the orbit, the separation between the two stars changes as a function of phase, implying a change in the wwc shock cone geometry. For example, the stagnation point changes from 30 $R_\odot$ at periastron to 56 $R_\odot$ at apastron. Depending on star B's wind velocity law, these distances might not be large enough for the wind to have attained $v_\infty$. Thus, the line-emitting region of star B might be truncated by the shock cone's limiting presence.

The possible wwc geometry on 1994 December 31, corresponding to spectrum swp53226 is shown

in Figure 22. The parameters used for this figure are $\dot{M}_A = 1{\times}10^{-3}\ M_\odot\ \mathrm{yr}^{-1}$, $v_\infty(\mathrm{A}) = 600$ km s$^{-1}$ and $R_A = 48\ R_\odot$ (from Koenigsberger et al. 1998b), $\dot{M}_B = 2{\times}10^{-5}\ M_\odot\ \mathrm{yr}^{-1}$ (assumed), and $v_\infty(\mathrm{B}) = 2600$ km s$^{-1}$. The shock cone is considerably narrower in this case, as expected given the very large mass-loss rate of star A, but at $\phi \sim 0.4$ there is still a large portion of WR wind projected on the core of star A, hence giving rise to a wind eclipse as speculated in § 3.3 to be the cause of the very weak N V 1240 Å line in this spectrum. The shape of the shock cone near the stagnation point, $R_0$, is not correctly represented in this figure because $R_0$ is merely $\sim 3\ R_\odot$ (periastron) to $20\ R_\odot$ (apastron) above the surface of star B, where the wind is expected to be still accelerating. Furthermore, "radiative braking" effects (Gayley et al. 1997) in the vicinity of star B are expected to be strong, thus lifting the wwc shock cone surface above the location that is predicted without the inclusion of radiative forces. Indeed, the fact that the underlying He II 1640 Å emission line that we believe belongs to star B is not severely distorted in swp53226 indicates that the He II line-forming region is not truncated by the shock, and thus, that "radiative braking" appears to be a strong effect.

Coriolis forces have also been neglected in the calculations shown in Figs. 20–22. To first order, Coriolis forces produce a rotation of the wwc shock cone axis by $\alpha$ degrees with respect to the axis joining the two stars, $\alpha \sim \tan^{-1}\ (v_{orb}/v_{wind})$, where $v_{orb}$ is the orbital velocity of one star with respect to the other, and $v_{wind}$ is the wind velocity. For $v_{wind} = 1700$ km s$^{-1}$ and $v_{orb} = 360$ km s$^{-1}$, $\alpha \sim 12°$.

### 5.2. *Velocities along the Shock Cone Walls*

The different symbols along the shock cone walls in Fig. 20 indicate locations for which tangential velocities were computed, and some of these values are noted. The maximum value of $v_t(\theta)$ depends strongly on the shock cone opening angle and on the values of $v_\infty$. For the cases illustrated in Fig. 20, $v_t(\theta) < 1000$ km s$^{-1}$ for all wwc regions closer than $10\ R_*(\mathrm{B})$, where wind densities are largest.

The line-of-sight component of $v_t$ corresponds to a position on the observed emission-line profiles. With the objective of determining the wavelengths within the observed line profiles where wwc effects might be expected, a simple calculation of the line profiles uses the line-of-sight velocity and an estimate of the emissivity along the shock regions. At this stage, given the scant available information on the temperature and density structure of the shock regions, the simplest assumption is that the excess emission arising from the wwc originates from the kinetic energy of the stellar winds. Thus, the emissivity of the wwc shock region is assumed to be proportional to the local wind density (which falls off as $r^{-2}$ once $v_{wind} \sim v_\infty$). Since the origin of the coordinate system is centered on the star with the weaker wind (star B, in this case), the density would correspond to that of this star's wind. The actual intensities, however, are in arbitrary units since our only concern is the wavelength range over which the wwc emission may contribute, as a function of orbital phase.

In Figure 23 these density profiles are compared with the *HST* line profiles of N IV] 1486 Å. As already mentioned, this line is less affected by absorption than are lines arising from permitted transitions, and it is a line clearly associated with star A. The N IV] 1486 Å line was corrected for the orbital motion of star A and for the assumed velocity of the SMC (+150 km s$^{-1}$) in HD 5980's neighborhood. Except for phases near the elongations, the wwc density profiles are highly asymmetrical, and it is, indeed, possible to associate the extended wings of these profiles with features on the extended wings of the observed profiles, particularly if "turbulent" motions of $\sim 500$ km s$^{-1}$ are assumed. However, large portions of the observed line profile cannot be associated with wwc emission, for example, the entire red half of the emission at $\phi = 0.36$, since no wwc emission is predicted for these velocites. It is important to note that the wwc density profiles are different from the actual emission line profiles that may arise in the wwc region, even under the simple density distribution assumed here. This is because the temperature of the gas contained within the two shocks that form the wwc shock cone walls depends strongly on the energy of the collision and the cooling function, and both of these quantities are expected to vary with distance. Hence, it is conceivable that only regions at large $\theta$ actually emit significant line radiation at optical/UV wavelengths, while the region near the stagnation point emits primarily X-rays. However, the main conclusion is that the N IV] 1486 Å line profiles do not exclude a contribution from wwc emission, but wwc emission cannot account for the entire emission-line profile.

## 6. EVOLUTIONARY STATUS OF HD 5980

Langer(1994) found that very massive single stars and case B mass-transfer primaries in binaries evolve identically, as long as effects of angular momentum

TABLE 5

ESTIMATED PARAMETERS OF HD 5980

| Parameter | 1979-81 | 1994 | 1999-2002 |
|---|---|---|---|
| $P_{orb}$ (days) | 19.2654 | ··· | ··· |
| Orbital inclination | 86[a] | ··· | ··· |
| a $/R_\odot$ | 127[b] | ··· | ··· |
| e | 0.3 | ··· | ··· |
| $M_{\rm StarA}/M_\odot$ | 50[b] | ··· | ··· |
| $M_{\rm StarB}/M_\odot$ | 28[b] | ··· | ··· |
| $V$(system) | −7.3[a] | −8.7[e] | −7.6[h] |
| $V$(eruptor=Star A) | −6.3 | −8.6[e] | −6.5 |
| $V$(Star B) | −5.8 | ··· | ··· |
| $V$(Star C) | −6.1 | ··· | ··· |
| $R_{\rm StarA}/R_\odot$ | 21[a] | $> 160$[d] | ··· |
| | ··· | 280[g] | ··· |
| $R_{\rm StarB}/R_\odot$ | 15[a] | ··· | ··· |
| $R_{\rm envStarB}/R_\odot$ | 30–40[a] | ··· | ··· |
| $v_\infty$(Star A)/(km s$^{-1}$) | ··· | 300–1700 | 1740–2200: |
| | ··· | 500[g] | ··· |
| $v_\infty$(Star B)/km s$^{-1}$ | 3100: | ··· | 2600–3100: |
| $v_\infty$(Star C)/km s$^{-1}$ | ··· | ··· | 1700:: |
| N[He]/N[H][aa]$_{\rm Non-LTE}$ | ··· | 0.4[e] | ··· |
| $\dot{M}/M_\odot$ yr$^{-1}$ | ··· | $10^{-3}$[e] | ··· |
| $L_{\rm StarA}/L_\odot$ | ··· | $3 \times 10^6$[e] | ··· |
| | ··· | $10^7$[g] | ··· |
| $T_*$(Star A) (°K) | 53,000[c] | 21,000[d] | ··· |
| | ··· | 35,500[e] | ··· |
| Spectrum (Star A) | WN3[b] | $B1.5Ia^+$[d] | WN6[d] |
| Spectrum (Star B) | WN4[b] | WN4: | WN4: |
| Spectrum (Star C) | ··· | ··· | O4-6[f] |
| $V_{rot}^A \, sin \, i$ (km s$^{-1}$) | ··· | ··· | 250::[j] |
| $V_{rot}^C \, sin \, i$ (km s$^{-1}$) | ··· | ··· | 75[i] |

[aa]Abundance ratio by number (0.63 by mass); [a]Breysacher & Perrier 1991; [b]Niemela et al. 1997; [c]Assuming $L_{\rm starA}$ $(L_\odot)$=const and $R_{\rm starA}/R_\odot = 21$; [d]Koenigsberger et al. 1998a; [e]December 30, Koenigsberger et al. 1998b; [f]Koenigsberger et al. 2000; [g]Drissen et al. 2001; [h]S. Duffau, adopting m-M = 19.1; [i]Koenigsberger et al. 2001; [j]Georgiev & Koenigsberger 2004a.



and internal rotation on the evolution are negligible. Rotation has a major effect on stellar evolution (Meynet et al. 1994; Meynet & Maeder 2000; Heger et al. 2000) and thus, if the presence of a companion affects its rotation properties, one may expect significantly different evolution in the binary stars than in their single-star counterparts. The interplay between mass transfer and stellar rotation is just starting to produce results that may be compared with observations (Wellstein, Langer, & Braun 2001; Petrovic & Langer 2004). In this section, the question of HD 5980's position on the H-R diagram will be addressed, and the constraints on its evolutionary status enunciated. As a first step, non-rotating star evolutionary tracks are used. The assumptions made and the parameters adopted are the following:

1. The current masses of star A and star B are, respectively, 50 and 28 $M_\odot$, based on the RV curves of Niemela et al. (1997).

2. In 1978, the stellar radii of star A and B are, respectively, 21 and 15 $R_\odot$ and the visual bright-

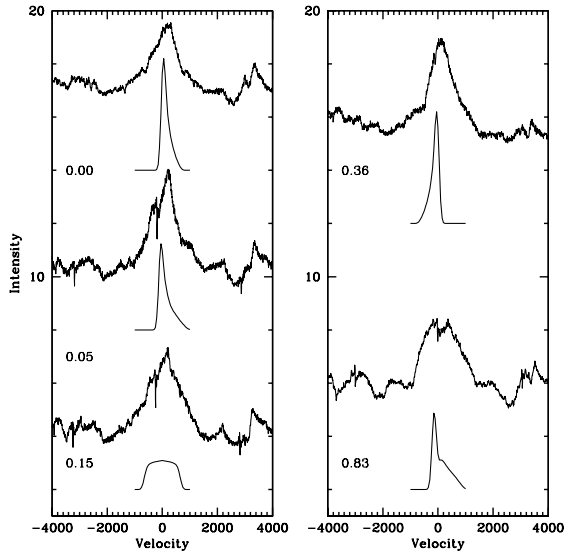


Fig. 23. Predicted line profiles arising from the wwc shock region, computed with $\dot{M}_A$, $\dot{M}_B$ = 50, $2\times10^{-5}$ $M_\odot$ yr$^{-1}$, and $v_\infty$(A), $v_\infty$(B) = 1700, 2600 km s$^{-1}$, compared with the observed line profiles of N IV] 1486 Å in the *HST* data. The predicted contribution from the wwc region is constrained to velocities slower than 1000 km s$^{-1}$.

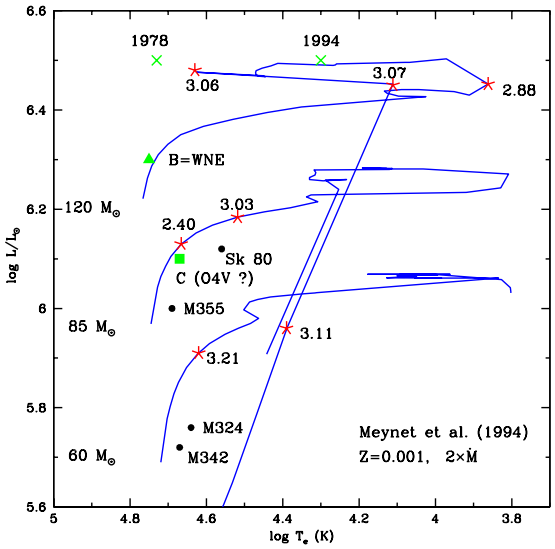


Fig. 24. Possible location of each of the three stars in HD 5980 on the HR diagram: star A (crosses), star B (triangle) and star C (square). Other stars associated with NGC 346 are noted. Evolutionary tracks are from Meynet et al. (1994); some of the ages are indicated with stars.

ness ratios of the three stars (A, B, and C, respectively) in the system are 0.41, 0.26, and 0.33 based on the light curve solution of BP90. In subsequent years, only star A undergoes changes in these parameters. The primary caveat with the $R_*$ values is that their derivation relies on the assumption that only star B had an extended envelope. A second consideration is the possibility that star A is strongly distorted due to rotation or tidal forces, and this, too, would affect the radii determination.

3. From the above brightness ratios, and using $E(B-V) = 0.07$, $m_{v(system)} = 11.7$ mag, and a reddening correction $a_\nu = 0.1$ mag, $m_{v(A)} = 12.57$ (1978), $m_{v(B)} = 13.08$, and $m_{v(C)} = 12.79$ mag. With a distance modulus to the SMC of 19.1 (MPG 1989), the absolute visual magnitudes are $V_A = -6.5$, $V_B = -6.0$, and $V_C = -6.3$ mag.

4. The luminosity of star A, $\log(L_A/L_\odot) = 6.5$, is adopted from Koenigsberger et al. (1998b), and is assumed to be constant over the time-period for which UV data are available. This luminosity is consistent with an assumed WNE classification (BC$\sim -5$ mag) and corresponds to $V_A = -6.5$ mag as obtained from the visual magnitudes. Near eruption maximum, however, Drissen et al. derived a larger luminosity, $\log(L_A/L_\odot) \sim 7$, based on different model calculations. It will be assumed, however, that the luminosity has remained constant over the recent years. Star C is assumed to be O4, based on the analysis of photospheric absorption lines by Koenigsberger et al. (2002), which implies a bolometric correction of BC = $-4.21$ mag if O4V, or BC = $-3.93$ mag if O4I, yielding $\log(L_C/L_\odot) = 6.1$ (O4V) or 6.0 (O4I), using the solar bolometric magnitude $M_\odot^{bol} = 4.79$ mag. The largest uncertainty is associated with star B. If it is a WNE star, then, following MPG, a "moderate" assumption is BC = $-5$ mag, leading to $\log(L_B/L_\odot) = 6.3$. This luminosity is far larger than that of any known or predicted H-free WNE star (Langer et al. 1994). If, however, star B is not a WNE

star, its luminosity would be much lower (for example, if it were O7 V, BC = −3.77, and $\log(L_B/L_\odot) = 5.82$) but given the discussion of § 3.3, the WNE type is, for the time being, favored.

5. The effective temperature of star A, $T_A$ = 21,000 K for 23 November 1994, is adopted from Koenigsberger et al. (1996), based on similarities with a B1.5Ia$^+$ spectrum. Assuming constant luminosity, and adopting $R_A = 21\ R_\odot$, then $T_A$ = 53,000 K in 1978, consistent with a WNE classification. For star C, $T_{\rm eff}$ = 46,500 (O4V) or 42,400 (O4I). Once again, the largest uncertainty is for star B. Assuming it is a WNE star ($\log(L_B/L_\odot) = 6.3$) and adopting $R_B = 15\ R_\odot$ implies $T_{\rm eff}$ = 56,000 K. But if it is not a WNE, and assuming as above the luminosity corresponding to a BC of an O7V star, then $T_{\rm eff}$ = 42,000 K.

6. The relative helium to hydrogen abundance by mass of HD 5980 is Y/X ∼ 0.63, from the NLTE analysis of the optical emission-line spectrum obtained on 31 Dec. 1994. Since this spectrum is dominated by the erupting star's spectral distribution, this abundance ratio can be taken to correspond to that of star A. For star B, a H-abundance X ∼ 0 is tentatively adopted.

Figure 24 illustrates the upper portion of the theoretical HR diagram constructed with evolutionary tracks from Meynet et al. (1994). These models correspond to low metallicity, Z = 0.001, and assume high mass-loss rates during the main sequence and WNL phases. The ages at a few locations along the tracks (in millions of years and marked with star symbols) are indicated.

Some of the most luminous stars of the NGC 346 cluster are also plotted in this diagram (filled circles), using data taken from MPG89 (their Table XI). Sk 80 (O7If) is the second most luminous star of the cluster and it is located relatively close to HD 5980 in the sky. Its location on the HRD suggests a ZAMS mass between 60 and 85 $M_\odot$, and a current age slightly larger than 3 million years. MPG 355 was classified as O3V((f*)) by MPG89, but Walborn et al. (2000) found nitrogen enhancements, and reclassified it as ON3III(f*). It is the fourth most luminous star, and its position on the HRD suggests a ZAMS mass somewhat lower than that of Sk 80.

The locations of the three members of the HD 5980 system are indicated in Fig. 24 as follows: star A with crosses; star B with a triangle; and star C with a square. Both star A and star B lie along the evolutionary track of a $M_{ZAMS} = 120\ M_\odot$ star. The two locations noted for star A correspond to 1994 December (declining portion of the eruption light curve) and 1978. Assuming that star B is an H-poor WN star, it must be the most evolved star of the HD 5980 system. Hence it must have originally been more massive than star A. Taken at face value, the location of star A implies that it evolved from a $M_{ZAMS} = 120\ M_\odot$ and that its current age is in the range 2.88–3.06 million years. However, according to the evolutionary track it is on, its current mass and location on the HRD would imply a zero hydrogen abundance, which is not consistent with the H-abundance obtained from observations. There are several possibilities to explain this contradiction. The first possibility is that the progenitor of star A was a less massive star that has evolved according to a rapidly rotating evolutionary model. The use of non-rotating tracks may overestimate the mass of the stars by as much as 50% (Maeder & Meynet 2001). Rotational mixing brings fresh H-fuel into the convective core, leading to a more massive core, which produces higher luminosities than the non-rotating stellar models (Talon et al. 1997; Heger, Langer, & Woosley 2000). Thus, the luminosity of star A may have increased significantly during the post-main sequence phases and the H-rich layers have not yet been removed. The second possibility is that star A accreted a large amount of H-rich gas when star B left the main sequence prior to becoming a WNE. A third, but very non-standard scenario may be envisioned in which star B is not a WNE but an O-type star that is accreting material from star A (which would be very H-poor), and which at the same time is ejecting part of the accreted gas mixed with its own H-rich layers. Indeed, one of the scenarios put forth to explain the LBV eruptions involves such a mass accretion process (see review by Gallagher 1989). It is not easy to reconcile the WNE characteristics of star B with this type of scenario, although very little is known about the expected characteristics of an accreting O-type star.

## 7. SUMMARY AND CONCLUSIONS

HD 5980 is a multiple system containing a close binary pair, in which an LBV-like eruption recently took place. In order to understand the mechanism that was responsible for the eruption and in order to

determine the evolutionary status of its stellar components, it is necessary to establish the nature of the stars involved, and this can only be done through an understanding of their spectral characteristics. In particular, the variability observed in the emission line profiles has a direct impact on the determination of the stellar masses through its effect on the radial velocity curves. The variability can be attributed primarily to the effects produced by physical and wind eclipses, with an additional contribution due to wind-wind collisions. Hence, one of the first steps required for understanding HD 5980 has been to determine the plausible characteristics of the winds, in order to estimate the degree to which wind eclipses and wind-wind collisions play a role in producing line profile variability. Fortunately, the binary system is an eclipsing system, allowing the use of the orbital phase-dependent variability of P Cygni absorption components for estimating the wind velocities of each of the two stars. A preliminary analysis yields $v_\infty$(A) $\sim$ 1700–2200 km s$^{-1}$ and $v_\infty$(B) $\sim$ 2600–3100 km s$^{-1}$ from data obtained during 1989/91, 1995, and 1999/2001. The ranges in these values reflect both the uncertainty in the interpretation of the observations and the fact that epoch- and phase-dependent variations are difficult to follow with the limited number of UV observations that are available. Having established these limits, however, an approach using model calculations to fit the profiles should narrow down these ranges, as well as provide a determination of the mass-loss rates.

One of the major questions that has recently been raised regarding HD 5980 concerns the nature of the secondary component, star B, and the possibility that it is not a WNE star as originally classified, since the WR-like emission lines could arise in a wind-wind collision region. The analysis of the wind-wind collision geometry under the thin shock approximation leads to the conclusion that the wind-wind collision shock cone is folded around star B during all epochs following 1989. According to the simple wwc model used here, although portions of the observed line profiles may contain contributions from the wwc region, the profiles as a whole are not consistent with an origin in the gas flowing along the shock cone walls. Hence, the emission lines must be primarily associated with the stellar winds of each star. Furthermore, four lines of evidence are presented that strongly suggest that star B possesses a very fast and dense stellar wind, with a high degree of ionization, consistent with the WNE hypothesis.

Using the parameters that have thus far been determined or estimated for HD 5980 and summarized in Table 5, the location on the H-R Diagram of its three components indicates that the progenitor of the A+B pair could have been a very massive binary system ($M_{ZAMS} \geq 120\ M_\odot$), under standard evolutionary scenarios, and that the system's age is $\sim$ 3 Myr. According to the tentative conclusion that the binary pair is LBV+WNE, then star B ( = WNE) is well on the way to becoming a supernova. However, the standard evolutionary scenarios predict a much smaller H-abundance than currently observed. Thus I conclude that the star A+star B binary pair is most likely the result of evolution with mass transfer and/or evolution with rapid rotation. It is also important to keep in mind that the evolutionary status of stars A and B relies completely on the mass determination derived from the RV variations curves of emission lines. Thus, until the distortion of the radial velocity curves due to wind eclipses and wwc's is quantified, the values of the masses cannot be fully established. In addition, in order to firmly establish whether star B is truly a WNE star, further abundance determinations of H (at different orbital phases and epochs) as well as a determination of the N abundance are necessary.

The study of HD 5980 raises a large number of questions that are relevant not only for gaining an understanding of this particular system, but also of binary systems with strong stellar winds, eccentric orbits or in advanced stages of evolution (see van der Hucht 2001 for a sample of such systems). The following are some of the questions that the present-day theoretical models may be in a position to answer:

1. What is the quantitative effect on the line profiles due to wind eclipses and wind-wind collisions? Is the effect large enough to lead to erroneous mass determinations?

2. What is the effect of periastron passage on the wind structure of the stars? Does the effect involve a variation in the mass-loss rate?

3. Given the timescales and the characteristics of the 1993-1994 eruptions in HD 5380, what are the constraints that can be placed on the mechanisms responsible for the instability that produced the eruption? Is it binary-related?

4. What is the origin of the rapid line-profile variability observed in 1999 apparently arising in star B? Is it associated with the recently detected polarization variations (Villar-Sbaffi et al. 2003)?

5. Star A may be the result of a prior mass-transfer event at the time when star B became a WR. Do the characteristics of star A correspond to those expected from such a mass-transfer phase?

I wish to express my gratitude to J. Cantó, K. Gayley, L. Georgiev, and W. Schmutz for many fruitful discussions; to N. Walborn, O. de Marco, and L. Smith for allowing use of the 1973 digitized data; to J. Petrovic for discussing with me the new mass-transfer evolutionary models; to A. Jones for providing the photometric data of HD 5980; to S. Duffau for providing a determination of the visual magnitude of HD 5980 in 2002; to M. López for help in producing Figure 4; to A. Díaz Azuara, C. Guzmán, E. Sacristán, G. Zavala, L. Hernández, and R. García for computing support; and to the referee, G. Graefner, for his valuable comments and suggestions. This investigation made extensive use of the Multimission Archive at the Space Telescope (MAST) and the NASA Astrophysical Data System (ADS) and was supported by CONACYT grant 36569E and UNAM/DGAPA/PAPIIT grant IN118202. STScI is operated by AURA, under NASA contract NAS5-26555.



## REFERENCES

Auer, L. H., & Koenigsberger, G. 1994, ApJ, 436, 859
Azzopardi, M., & Vigneau, J. 1975, A&AS 22, 285
Barbá, R. H., Morrell, N. I., Niemela, V. S., et al. 1996, in RevMexAASC, 5, Workshop on Colliding Winds in Binary Stars to honor Jorge Sahade, eds. V. Niemela & Nidia Morrell (Mexico City: Inst. Astron., UNAM), 85
Barbá, R., & Niemela, V. S. 1995, in IAU Symp. 163, Wolf-Rayet Stars: Binaries, Colliding Winds, Evolution, eds. K. A. van der Hucht & P. M. Williams (Dordrecht: Kluwer), 254
Barbá, R., Niemela, V. S., Baume, G., & Vázquez, R. A. 1995, ApJ, 446, L23
Barbá, R., Niemela, V. S., & Morrell, N. 1997, in ASP Conf. Ser. Vol. 120, Luminous Blue Variables: Massive Stars in Transition, eds. A. Nota & H. Lamers (San Francisco: ASP), 238
Bateson, F. M., Gilmore, A., & Jones, A. F. 1994, IAU Circ., 6102
Bateson, F. M., & Jones, A. 1994, Publ. Var. Star. Sec. R. Astron. Soc. New Zealand, 19
Breysacher, J. 1997, in ASP Conf. Ser. 120, Luminous Blue Variables: Massive Stars in Transition, eds. A. Nota & H. Lamers (San Francisco: ASP), 227
Breysacher, J., Moffat, A. F. J., & Niemela, V. 1982, ApJ, 257, 116 (BMN82)
Breysacher, J., & Perrier, C. 1980, A&A, 90,207 (BP80)
_____. 1991, in IAU Symp. 143, Wolf Rayet Stars and Interrelations with other Massive Stars in Galaxies, eds. K. van der Hucht & B. Hidayat (Dordrecht: Kluwer), 229 (BP91)
Breysacher, J., & Westerlund, B. E. 1978, A&A, 67, 261
Cantó, J., Wilkin, F., & Raga, A. C. 1996, ApJ, 469, 729
Conti, P.S. 1984, in IAU Symp. 105, Observational Tests of the Stellar Evolution Theory, eds. A. Maeder & A. Renzini (Dordrecht: Reidel), 233
Crowther, P. A., & Dessart, L. 1998, MNRAS, 296, 622
Davidson, K., Moffat, A. F.J ., & Lamers H. J. G. L. M., 1989, in IAU Coll. 113, Physics of Luminous Blue Variables, Astrophysics and Space Science Library Vol. 157 (Dordrecht: Kluwer)
de Boer, K. S., & Savage, B. D. 1980, ApJ, 238, 86
Drissen, L., Crowther, P. A., Smith, L. J., Robert, C., Roy, J.-R., & Hillier, D. J. 2001, ApJ, 545, 484
Feast, M. W.,Thackeray, A. D., & Wesselink, A. F. 1960, MNRAS, 121
Gallagher, J. 1989, in IAU Coll. 113, Physics of Luminous Blue Variables, Astrophys. and Space Science Library (Dordrecht: Kluwer), 185
Gayley, K. G, Owocki, S. P., & Cranmer, S. R. 1997, ApJ, 475, 786
Georgiev, L., & Koenigsberger, G. 2004a, in IAU Symp. 215, Stellar Rotation, eds. A. Maeder & P. Eenens, in press
_____. 2004b, A&A, in press
Heger, A., Langer, N., & Woosley S. E. 2000, ApJ, 528, 368
Heydari-Malayari, M., Courbin, F., Raauw, G., Esslinger, O., & Magain, P. 1997, A&A, 326, 143
Hoffmann, M., Stift, M. J., & Moffat, A. F. J. 1978, PASP, 90, 101
Humphreys, R., & Davidson, K. 1994, Review on LBV's
Jones, A. F., & Sterken, C. 1997, Astronomical Data 3, 4
Kaufer, A., Schmid, H. M., Schweickhardt, J., & Tubbesing, S. 2002, in ASP Conf. Ser. Vol. 260, Interacting Winds from Massive Stars eds. A. F. J. Moffat & n. St.-Louis (San Francisco: ASP), 489
Koenigsberger, G. & Auer, L.H. 1985, ApJ, 297, 255
Koenigsberger, G., Auer, L. H., Cardona, O., Drissen, L., Moffat, A. F. J., St.-Louis, N., & Seggewiss, W. 1993, in ASP Conf. Ser. 35, Massive Stars: Their Lives in the Interstellar Medium, eds. J. P. Cassinelli & E.B. Churchwell (San Francisco: ASP), 249
Koenigsberger, G., Auer, L. H ., Georgiev, L., & Guinan, E. 1998a, ApJ, 496
Koenigsberger, G.,, Georgiev, L., Barbá, R., Tzvetanov, Z., Walborn, N. R.,Niemela, V., Morrell, N., & Schulte-Ladbeck, R. 2000, ApJ, 542, 428
Koenigsberger, G., Georgiev, L., Peimbert, M., Walborn, N. R., Barbá, R., Niemela, V., Morrell, N., Tzvetanov,Z., & Schulte-Ladbeck, R. 2001, AJ, 121, 267
Koenigsberger, G., Guinan, E., Auer, L. H., & Georgiev,

L. 1995, ApJ, 452, 107
Koenigsberger, G., Kurucz, R. L., & Georgiev, L. 2002, ApJ, 581, 598
Koenigsberger, G., Moffat, A. F. J., St. Louis, N., Auer, L. H., Drissen, L., & Seggewiss, W. 1994, ApJ, 436, 301
Koenigsberger, G., Peña, M., Schmutz, W., & Ayala, S. 1998b, ApJ, 499, 889
Koenisberger, G., Shore, S. S., Guinan, E., & Auer, L. H . 1996, RevMexAASC, 5, Workshop on Colliding Winds in Binary Stars to honor Jorge Sahade, eds. V. Niemela & Nidia Morrell (Mexico City: Inst. Astron., UNAM), 92
Langer, N. 1994, in IAU Symp. 163, Wolf-Rayet Stars: Binaries, Colliding Winds, Evolution, eds. K. A. van der Hucht & P. M. Williams (Dordrecht: Kluwer), 15
Langer, N., Hamann, W.-R., Lennon, M., Najarro, F., Pauldrach, A. W. A., & Puls, J. 1994, A&A, 290, 819
Maeder, A., & Meynet, G. 1987, 182, 243
Maeder & Meynet 2001, A&A 373,555
Massey, P. 2003, ARA&A, 41, 15
Massey, P., Parker, J. W., & Garmany, C. D. 1989, AJ, 98, 1305
Meynet, G., & Maeder, A. 2000, A&A, 361, 101
Meynet, G., Maeder, A., Schaller, G., Schaerer, D., & Charbonnel, C. 1994, A&AS, 103, 97
Moffat, A. F. J., Koenigsberger, G., & Auer, L. H. 1989, ApJ, 344, 734
Moffat, A. F. J., Marchenko, S. V., Bartzakos, P., et al. 1998, ApJ, 497, 896
Niemela, V. S. 1988, in ASP Conf. Ser. Vol. 1, Progress and Opportunities in Southern Hemisphere Optical Astronomy. The CTIO 25th Anniversary Symposium, eds. V. M. Blanco & M. M. Phillips (San Francisco: ASP), 381
Niemela, V. S., Barbá, R. H., Morrell, N. I., & Corti, M. 1997, in ASP Conf Ser. Vol. 120, Luminous Blue Variables: Massive Stars in Transition, eds. A. Nota & H. Lamers (San Francisco: ASP), 222
Niemela, V. S., Barbá, R., & Morrell, N. 1998, Highlights of Astronomy Vol. 11A, presented at Joint Discussion 14 of the XXIIIrd General Assembly of the IAU, ed. J. Andersen (Dordrecht: Kluwer), 365
Nota, A., & Leitherer, C. 1997, LBV Symposium Kona
Petrovic, J., & Langer, N. 2004, IAU Coll. 194, Compact Binaries in the Galaxy and Beyond, in press
Prinja, R. K., Barlow, M. J., & Howarth, I. D. 1990, ApJ, 361, 607
Savage, B. D., & de Boer, K. S. 1981, ApJ, 243, 460
Smith, L. 1997, in ASP Conf Ser Vol. 120, Luminous Blue Variables: Massive Stars in Transition, eds. A. Nota & H. Lamers (San Francisco: ASP), 245
Stahl, O., Jankovics, I., Kovács, J,. et al. 2001, A&A, 375, 54
Stahl, O., Wolf, B., Klare, G., et al. 1983, A&A, 127, 49
van den Bergh, S. 1976, IAU Circ. No. 2993
van der Hucht, K. A. 2001, New Astron. Rev., 45, 135
Villar-Sbaffi, A., Moffat, A.F.J., St.-Louis, N., 2003, ApJ 590, 483
Walborn, N. R. 1977, ApJ, 215, 53
Walborn, N. R., Lennon, D. J., Heap, S. R., Lindler, D. J., Smith, L.J ., Evans, C. J., Parker, J. W. 2000, PASP, 112, 1243
Walborn, N. R., Nichols-Bohlin, J., & Panek, R. J. 1980, *IUE* Atlas of O-type Spectra from 1200 to 1900 Angstroms, NASA
Wellstein, S., Langer, N., & Braun H. 2001, A&A, 369, 939
Westerlund, B. H. 1997, The Magellanic Clouds (Cambridge: CUP)
Willis, A. J., et al. 1979, in The First Year of IUE, ed. A. J. Willis (London: University College), 394



Gloria Koenigsberger: Centro de Ciencias Físicas, UNAM, Apdo. Postal 48-3, 62251 Cuernavaca, Morelos, México (gloria@astroscu.unam.mx).